Author/s:
Harris, AR;Wallace, GG

Title:
Organic Electrodes and Communications with Excitable Cells

Date:
2018-03-21

Citation:
Harris, A. R. & Wallace, G. G. (2018). Organic Electrodes and Communications with Excitable Cells. Advanced Functional Materials, 28 (12), https://doi.org/10.1002/adfm.201700587.

Persistent Link:
https://hdl.handle.net/11343/261092

DOI: 10.1002/adfm.201700587

Article type: Feature Article

Organic Electrodes and Communications with Excitable Cells

Alexander R. Harris, Gordon G. Wallace**

Dr. A. R. Harris, Prof. G. G. Wallace

ARC Center of Excellence for Electromaterials Science, Intelligent Polymer Research Institute, University of Wollongong, NSW 2522, Australia.

Email: alexrharris@gmail.com; gwallace@uow.edu.au

Abstract

Electrodes can provide information on neural function and stimulate neural activity. These neural electrodes can provide remarkable benefit to people suffering physical trauma or neural disease. Traditional metal electrodes have shortcomings related to poor biostability, cytocompatibility and a rigid structure that maps poorly to tissue. Organic conductors can be formed with various chemical and physical properties to create improved electrode-neural interfaces. The processability of organic conductors enables their use in advanced fabrication methods. This review details the use of graphene, carbon nanotubes and conducting polymers for neural interfacing. Construction of novel neural electrode architectures via advanced fabrication processes is also addressed.

1. Introduction

Our ability to communicate with neuronal cells underpins our understanding of neural disease,[1] the ability to monitor the onset of biological abnormalities such as epileptic seizures[2] or to provide functionality in cases of physical trauma such as severed nerves.[3] The use of stimulation to promote arborisation may also have a role to play in treating neuronal diseases such as schizophrenia[4] or neural degenerative diseases such as Alzheimer's.[5] As we develop more accurate neural stimulation systems, the targeting of particular nerves to treat specific diseases has become of interest, giving rise to the field of electroceuticals.[6] As robotics improve, effective interfacing of the nervous system with externally driven prosthetics is also rapidly developing, providing benefit to patients who have lost limbs, suffer spinal cord injuries, had a stroke or suffer locked-in syndromes such as amyotrophic lateral sclerosis (ALS) or multiple sclerosis (MS).[7] High fidelity communication with neuronal cells will ensure success in each of these important areas. Such fidelity is critically dependent on the electrode – cellular interface[8] and hence the composition and physical form of the electrode materials used.

Nerve and muscle cells are electrically excitable, both producing and sensing electrical currents. The simplest and most common method for measuring and stimulating function of these cells is via an electrode. A conductive electrode in close proximity to the cells can detect fluctuations in local electrolyte concentration, generating changes in potential. Charge can also be injected from the electrode into the tissue, inducing neural stimulation. To date, the majority of electrodes used for clinical devices are platinum or platinum-iridium. While these materials have a high conductivity and are corrosion resistant, they have a number of shortcomings, including being very expensive precious metals. These metal conductors are hard and stiff so that relative movement of the soft, flexible

organic tissue in contact with the electrode can result in loss of contact with the target cells, tissue damage and scarring. The ability to alter composition and hence surface chemistry at the electrode-cellular interface is limited. The high melting point of the metals limits the physical form of electrodes that can be fabricated.

The development of conductive organic materials provides an important addition to the electromaterial inventory for neural communications. Organic conductors are inexpensive and are able to be synthesized in bulk quantities. The infinite variety of organic structures allows tailoring of the chemical composition and surface charge for optimal cytocompatibility. Different materials can be easily combined to produce complex structures and functionality that can be tailored for individual applications. The physical properties of the organic conductors can also be modified, leading to soft, flexible electronics that can float within or on-top-of the target tissue.

Another big advantage of organic conductors is their processability. The materials can be dispersed in a variety of solvents and used in numerous processing systems. Recent developments in advanced fabrication include additive manufacturing and fiber spinning, enabling formation of novel structures which traditional metalworking is incapable of producing. Now that the pathways for development of advanced materials and new fabrication tools have converged, our ability to create practically useful systems containing novel electromaterials for neuronal communications has been given a new lease of life.

Organic conductors such as graphene, carbon nanotubes and conducting polymers have demonstrated some extraordinary abilities in terms of communicating with neuronal cells. Previous reviews of this field have mainly focused on the materials used for neural tissue interfacing[9-12]. Here we provide details on the early work with each of these materials before discussing some of the latest progress with them. Unlike previous reviews, different fabrication methods are then addressed, highlighting some key publications on controlling material structure and their impact on cell behavior.

2. Organic Materials

2.1. Graphene

Graphite has long been mined and used for various applications, including as electrodes in batteries. The structure of crystalline graphite is multi-layers of hexagonal, aromatic carbon resulting in high conductivity along individual planes. Graphite is extremely low cost and light weight, and is amenable to physical or chemical treatments that can be used to tailor a range of properties. Natural graphite can contain impurities and defects that reduce electrical conductivity and may be toxic to cells[13]. Synthetic graphite removes issues of impurities, and highly oriented pyrolytic graphite (HOPG) is regularly used as a high quality electrode[14]. However graphite and HOPG are large, fragile, crystalline materials that are not suitable for interfacing with small, soft neurons.

2.1.1. Synthesis of Graphene-Based Materials

Thin layers of graphene have regularly been exfoliated from graphite[15], however in 2004, macroscopic single layers of graphene were obtained[16]. This work was rewarded with the Nobel Prize in Physics in 2010 and has resulted in a boom in graphene research. Graphene sheets possess high electrical conductivity in 2-dimensions, are thermally conductive, extremely strong, flexible and optically transparent. This has resulted in numerous reports of graphene electrodes for various applications.

Large sheets of graphene with minimal defects can be obtained by exfoliation, using adhesive tape or a sharp wedge to pare layers from graphite or HOPG. Chemical vapor deposition (CVD) also allows growth of high purity graphene. Numerous other methods for producing graphene of varying quality and size are available. These approaches have been covered in previous reviews[17]. Graphene is a highly hydrophobic material, limiting solubility in most solvents and hence processability. The introduction of functional groups renders graphene more dispersible, enabling further processing or chemical functionalisation. To generate graphene with oxygen containing groups attached, Hummers' method is typically used, where flake graphite is oxidized by $KMnO_4$, $NaNO_3$ and H_2SO_4[18]. The graphite oxide produced has a disrupted stacking, allowing solvent to penetrate the layers and forming

a dispersion of graphene oxide (GO) after sonication[19]. GO is an electrical insulator and can be reduced (rGO) by chemical, thermal or electrochemical methods to increase conductivity. However the reduction process is not complete, so that the rGO structure is not pure graphene.

2.1.2. Interfacing Graphene with Cells

A perspective article in 2012 discussed the ability of graphene, GO and rGO to interface with cells[20]. A more comprehensive review of carbon-based nanomaterials for tissue engineering was published in 2013, it included graphene, GO, rGO and some material composites, focusing on biocompatibility[9]. Another review in 2013 addressed neural recording and included the use of graphene modified electrodes[21]. In 2014, a major review of materials tested for neural implants was published[10]. This work included graphene, GO, rGO and their composites ability to record and stimulate neurons and the materials biocompatibility. We have recently published a comprehensive review of graphene, GO and rGO for bionics applications and tissue engineering[22].

Graphene has been used as a substrate for interfacing with different cell types, including human mesenchymal stem cells (hMSCs)[23], human neural stem cells (hNSCs)[24], human osteoblasts[23, 25], fibroblasts[26], myocytes[27], adenocalcinoma cells[28] and cell lines such as PC12[29].

Specific examples of different cell types growing on graphene, GO and rGO are detailed below. CVD grown graphene was adhered to a glass substrate and coated with laminin before culturing hNSCs[24]. The hNSCs adhered rapidly onto the graphene layer and then proliferated across the entire culture plate. Changing the culture media allowed cell differentiation to occur, and after 3 weeks, there was a difference in cell morphology on the glass compared to the graphene. After 4 weeks, there was a higher cell count on the graphene than the glass regions, indicating a more favorable substrate for cell attachment. Cell staining after differentiation revealed a higher number of neurons to glia on the graphene and the opposite response on the glass. Voltage pulses could then be passed through the graphene to electrically stimulate the adhered neurons, with calcium imaging confirming the electrical excitability of the cells.

Adult rat primary retinal ganglion cells were seeded onto graphene patterned glass and sapphire with or without a poly D-lysine and laminin coating[30]. After 6 days culture, neurite outgrowth was seen on all substrates. No difference in cell survival rates or cell body size was found on coated glass or graphene. There was a slight, statistically significant decrease in cell count and cell body size on bare graphene compared to glass. The neurite number and length was also reduced on the bare graphene in comparison to bare glass. This indicated cell adhesion may be reduced on the graphene, but the substrate was not cytotoxic. Culturing of postnatal day 7 retinal ganglion cells showed similar behavior, but with thicker cell processes, indicating the formation of neurite bundles. Patterning of the graphene allowed some control of the neurite growth. This work demonstrates that both newborn and adult neural cells are compatible with graphene. The peptide coating on a graphene electrode would be expected to dissolve or degrade when implanted, so the demonstration of compatibility of the bare graphene is critical.

Postnatal day 1 mouse hippocampal neurons were also grown on graphene with a poly L-lysine coating[31]. AFM measurement of the graphene gave a roughness of 4.49 nm, very similar to the underlying polystyrene culture dish. The contact angle of the graphene was 78.9°, slightly higher than the polystyrene at 61.2°, indicating the graphene is more hydrophobic. To remove any impurities from the graphene fabrication and to sterilize the substrate, the culture dish was soaked overnight in milli-Q water, then 12 hours in 75% ethanol, coated with poly L-lysine overnight, rinsed in water and finally soaked overnight in culture medium before seeding cells. There were no differences in cell number between the graphene and polystyrene after 7 days. The number and size of neurites increased with days of culture. Graphene produced a significant increase in neurite length compared to polystyrene.

rGO has also been used to interface with different cell types. GO was dispersed in methanol and spun onto a glass substrate before reduction with hydrazine[32]. The resulting films were essentially flat, with a roughness of 1.6 nm due to folds and wrinkling of the rGO sheets. PC12 cells attached and

proliferated well on the rGO with or without precoating with poly L-lysine. Human oligodendroglia and human fetal osteoblasts were also able to proliferate on the rGO.

Mouse induced pluripotent stem cells (iPSCs) were grown on GO or rGO coated coverslips[33]. Cells proliferated more on the GO than rGO. Cells on GO or glass spontaneously lost their pluripotency, while the rGO impeded differentiation. As the GO and rGO surfaces had similar roughness, the differences in cell differentiation are attributed to changes in hydrophilicity and oxygen functional groups.

2.1.3. Electrical Stimulation and Recording with Graphene

Graphene can be used to record the activity of excitable cells. Graphene can be formed into various electrode structures to interface with different cell types. Details of these are discussed. CVD grown graphene was patterned onto a flexible PDMS probe[34]. A steam plasma treatment could then be applied to functionalise the graphene and increase its hydrophilicity. Spontaneous activity was measured from the abdominal nerve cord of a crayfish. A signal-to-noise ratio (SNR) of 27.81 dB was recorded on the pristine graphene and a smaller 20.30 dB of the functionalised graphene. An electrocardiogram from a zebrafish was also acquired.

CVD grown graphene was transferred onto a flexible polyimide (Kapton) film with gold contacts. The graphene was patterned via photolithography and oxygen plasma etching before encapsulation with SU-8[35]. Some of the graphene was then treated with 70% nitric acid, where adsorption of NO_3^- resulted in p-type doping. The doped graphene had a one order of magnitude reduction in impedance (compared to undoped) at low frequencies, which would suppress electronic noise. It also had a larger capacitance, leading to higher charge injection capacity, with potential benefit for neural stimulation. A craniotomy was performed on a rat animal model, with the electrode placed on the cortex to perform electrocorticography (ECoG). Epileptiform activity was induced by application of bicuculline methiodide to the exposed brain region. The doped graphene electrode showed a 5-6 times reduction in noise compared to gold electrodes of the same size. Undoped graphene had a noise level intermediate between the doped graphene and gold electrodes. Recordings of spontaneous electroencephalography (EEG) in a feline model and somatosensory-evoked potential in an anaesthetised rat were also performed. Furthermore, the transparency of the graphene electrode allowed combined calcium imaging with neural recording of hippocampal slices.

Another graphene ECoG was patterned onto Parylene C and implanted in rat animal models (Figure 1)[36, 37]. The graphene had a slightly higher impedance and smaller charge injection capacity compared to platinum and gold electrodes. However these metal electrodes have a low light transmission, limiting their usefulness in combining electrical recording/stimulation with optical imaging, calcium imaging or optogenetic stimulation of cells. ITO is typically used for forming transparent electrodes for combined electrical and optical interrogation of neurons. The optical transmission of the 15 μm thick Parylene C with four layers of graphene was around 90%. This optical transmission is higher and over a wider range of wavelengths than on ITO. ITO is also a brittle material incompatible with complex folds of the cortical surface. In addition, ITO requires high fabrication temperatures, limiting the type of substrate that can be used and hence possible electrode geometries. Platinum and graphene electrodes were implanted into rats and both experienced an increase in impedance over the first 10 days but with no significant difference between electrodes. The electrodes showed similar baseline neural recordings and electrically evoked potentials when the sciatic nerve was stimulated. Electrodes were also placed into Thy1::ChR2 mice. Illumination of the cerebral cortex with blue light induced optogenetic stimulation of the neurons which was detected on the graphene electrodes. A cranial window was also implanted, allowing imaging of the cortex and cerebral vasculature and measuring 3D optical coherence tomography (OCT) beneath the implanted ECoG. The transparency of the graphene removed any imaging artefacts and masking that occurred with the opaque platinum electrodes.

Fibers of GO have been heat treated to form rGO before coating with parylene C (Figure 2)[38]. Laser ablation removed the parylene from the tip resulting in a rough and amorphous electrode. The electrode was able to stimulate explanted retinal ganglion cells. Coating the fiber with sucrose

increased its stiffness to enable insertion into the visual cortex; after the sucrose dissolved, neural recording could be performed.

Graphene-based materials can also be used to form field-effect transistors (FET) which have a lower noise level and higher sensitivity than recording electrodes. Yeast cells were grown on a rGO FET and exposed to alcohol[39]. The stressed cells compressed, leading to folding of the rGO and a decrease in FET conductance. Cardiomyocyte-like HL-1 cells were cultured on an array of graphene FETs[27]. The conductance of the graphene could be controlled by varying the gate voltage and enable a sensitivity one order of magnitude greater than other Si- or AlGaN-based devices. The cardiomyocytes propagated across the FET array and action potential propagation could be detected. Addition of norepinephrine increased the spike frequency.

2.1.4. Graphene Composites

Electrode composition can be manipulated by using graphene-based composite materials. However, in so doing fabrication options become more limited and so most, maybe all work in this area involves coating more conventional electrodes or using cytocompatible insulating substrates as described above. Several groups have reported that GO can be incorporated into conducting polymers. GO was dispersed in an aqueous solution with pyrrole (Py) and polystyrene sulfonate (PSS)[40]. Current was then passed through a platinum neural electrode to polymerise the pyrrole, forming a PSS and GO doped polypyrrole layer on the electrode surface (PPy/PSS/GO). The incorporation of the GO increased the surface roughness in comparison to PPy/PSS modified electrodes. The impedance of the electrodes at 1 kHz decreased from bare Pt > PPy/PSS > PPy/PSS/GO modified electrodes which is a predictor of the signal-to-noise ratio of the electrodes for neural recording. The charge injection capacity is important for neural stimulation and was measured via cyclic voltammetry with PPy/PSS/GO > PPy/PSS > bare Pt. In another demonstration, 3,4-ethylenedioxythiophene (EDOT) was dissolved with dispersed GO with subsequent electrochemical growth of poly(3,4-ethylenedioxythiophene) (PEDOT) doped with GO on platinum/iridium microelectrodes[41]. Rat cortical neurons were seeded onto the PEDOT/GO, with no significant difference in cell viability or cell numbers compared to PEDOT/PSS while the PEDOT/GO allowed formation of significantly longer neurites than the PEDOT/PSS. The GO of the modified electrodes was then covalently modified with a laminin fragment peptide P20 which resulted in even longer neurite growth (no electrical stimulation was used in this work). Other work demonstrated that PC12 and NIH/3T3 cells could proliferate on PEDOT-GO on gold electrodes[42].

Electrodes modified with graphene-based materials or their conducting polymer composites are still relatively hard. Hydrogels are polymeric materials that can contain over 90% water, and can be very soft and flexible. Polylactic acid (PLA) and polylactic-co-glycolic acid (PLGA) are two typical, biocompatible and biodegradable polymers made from the polymerization of lactic acid and glycolic acid. Mixtures of PLA and PLGA were drop cast onto CVD grown graphene[43]. PC12 cells were seeded on the graphene/hydrogel composite, with cell density highest on a 50:50 PLA/PLGA mixture. Cells were then differentiated and electrical stimulation led to a large increase in neurite length and connectivity. GO and carbon nanotubes can also be incorporated into hydrogels to support cell growth[44].

2.2. Carbon Nanotubes

Before large sheets of graphene were produced, fullerenes were discovered. Fullerenes are hollow graphene structures that can be shaped liked soccer balls (buckyballs) or long tubes (carbon nanotubes (CNT)). The discovery of buckyballs in 1985 led to the Nobel Prize in Chemistry in 1996[45]. Carbon nanotubes were subsequently synthesized in 1991[46]. CNTs can comprise a single layer of graphene to form single walled nanotubes (SWNTs) or multiple layers creating multi-walled nanotubes (MWNTs). CNTs are 1-dimensional materials with extremely high strength and thermal conductivity. The graphene sheets of SWNTs and MWNTs can be rolled at different angles and diameters which can alter the electrical characteristics of the nanotube giving metal or semiconductor properties.

2.2.1. Synthesis of Carbon Nanotubes

Fullerenes can be found naturally, but are highly irregular. They are typically synthesized via chemical vapor deposition from feed gases onto a substrate. This allows growth of highly uniform and aligned CNT mats. The substrate typically has a catalyst bed of cobalt, nickel or iron. The catalytic particle remains attached to the CNT after growth, and use of the as grown material may be toxic. Removal of the catalyst may be achieved by acid washing or oxidation, although this can introduce functionality into the CNT. Similar to graphene, CNTs have a very low solubility in most solvents. Functionalisation of the CNTs can enable their dispersion in solvents, but can impact on their structure and conductivity. The CNTs can be grown directly onto the target substrate which can be patterned. However the substrate must be heated to high temperatures for CVD, limiting the types of substrates that can be used. Transfer of CNTs can be achieved by transfer printing, applying tape to adhere to the CNTs, drawing the CNTs to form a fiber, or forming a dispersion and casting it onto another substrate. Depending on the growth and transfer method, individual CNTs can be obtained or multiple CNTs can form a vertically aligned mat, a random mesh, or fiber.

2.2.2. Interfacing Carbon Nanotubes with Cells

A number of reviews have been published previously which include CNT-neural interfaces[11]. A 2008 review discussed CNTs for neural implants including their biocompatibility[47]. In 2011, further details on modified CNTs and surface patterning were shown to affect neural growth and neural stem cell differentiation[48]. The 2013 and 2014 reviews of carbon-based materials for neural implants also included CNTs[9, 10, 21].

Reports of different cell types growing on various forms of CNTs include hippocampal cells[49-51], dorsal root ganglions (DRGs)[52], cortical and cerebellar neurons, fibroblasts, Schwann cells[53], osteoblasts[54], PC12s[55] and NG108-15 neuroblastoma-glial cells[56].

The first report of CNTs providing an effective interface with neurons was created by drop casting a dispersion of MWNTs onto glass coverslips[49]. The random mat of MWNTs allowed attachment and growth of rat hippocampal cells. Neurite outgrowth occurred, but was not directed. Modification of the MWNT with 4-hydroxynonenal (4-HNE) further increased the number and length of neurites. To obtain a more homogeneous surface coverage of MWNTs, as prepared MWNTs were functionalised with pyrrolidine groups, dispersed in dimethylformamide, drop cast onto glass slides and baked at 350°C in nitrogen atmosphere to defunctionalise the MWNTs[50]. Hippocampal neurons grew neurites and formed synapses which displayed an average 6-fold increase in spontaneous postsynaptic currents measured by patch clamping. MWNTs were also functionalized by refluxing in concentrated sulfuric and nitric acids for 6 hours before casting a random mat on polycarbonate and seeding DRG neurons[52]. The neurons sprouted longer neurites on the functionalized MWNT mat compared to non-functionalized MWNTs, indicating the oxygen functionality improves neurite adhesion and growth. SWNTs were modified with PEG to improve their solubility then spray coated onto glass slides and allowed growth of hippocampal neurons[57]. The surface charge of MWNTs was modified with various functional groups with more growth cones and longer neurites found on positively charged MWNTs than zwitterionic or negatively charged MWNTs[51]. Amino-functionalised MWNTs in the presence of nerve growth factor (NGF) also stimulated greater neurite growth than MWNTs or NGF on their own[55]. Human embryonic stem cells (hESCs) have been cultured on poly(acrylic acid) (PAA) modified CNT mats[58]. The hESCs showed strong differentiation towards neural lineage compared to glass substrates modified with PAA or poly L-ornithine. Layer-by-layer (LBL) assembly of poly(styrene-4-sulfonate) modified SWNTs and laminin was formed on a silicon oxide substrate which provided support for NSC growth and spontaneous differentiation[59]. LBL growth of PPy and MWNTs was also viable for PC12 growth[60].

Different CNT alignments can also be used to interface with cells. Vertically aligned MWNTs were functionalized by soaking in sulfuric and nitric acids. The functionalization of the MWNTs induced clumping, forming pyramidal or honeycomb like structures which supported fibroblast growth[61]. Vertically aligned MWNTs were coated with polypyrrole to form pyramidal structures, before soaking in collagen, allowing growth of PC12 cells[62]. MWNTs can also be drawn into aligned sheets and fibers, enabling growth of multiple cell types and some control of neurite direction[53]. MWNT sheets coated with PPy were used to grow myoblasts; myotubes aligning with the underlying MWNTs

(Figure 3)[63]. The PPy coating improved the cytocompatibility of the substrate, and electrical stimulation increased the cell density and myotube formation.

2.2.3. Electrical Stimulation and Recording with Carbon Nanotubes

Recording of neural activity with CNT modified electrodes has been demonstrated. CNTs were grown directly onto titanium nitride microelectrode arrays (MEAs), significantly increasing the charge density of the electrode[64]. High quality spontaneous action potentials were then detected from cultured cortical neurons. Bare MWNTs, acid chloride functionalized MWNTs and PPy modified MWNTs were attached to MEAs. The modified electrodes possessed higher charge injection capacity and lower impedances at 1 kHz compared to uncoated electrodes. Spontaneous action potentials were recorded from cortical neurons grown on the MWNT modified electrodes for up to 88 days. The stimulation threshold for the neurons was also lower on the modified electrodes. In vivo recording from rat motor cortex and monkey visual cortex was also performed, with higher signals recorded across the entire measurement frequency compared to bare metal electrodes[65]. Rabbit retinal ganglion cell activity has been recorded on SWNT bundles[66]. CNTs were grown on a flexible polyimide MEA and able to record activity from the tail of a crayfish or the surface of a rat motor cortex[67]. CNT bundles on a tungsten electrode recorded activity from mice brain[68]. Amino functionalized CNTs have also been used to record activity from crayfish neurons[69]. PEDOT-CNT electrodeposited on a microelectrode[70] could record multi-unit activity from a rat inferior colliculus[71], somatosensory cortex[72] and visual cortex for up to 4 months[73]. PEDOT-CNT could also be loaded with dexamethasone, an anti-inflammatory; electrical stimulation released the dexamethasone, reducing the inflammation area and improving neural health[74]. Vertically aligned CNTs were coated with boron doped diamond, significantly increasing the charge storage capacity and reducing the electrode impedance; they were also used to record and stimulate action potentials[75]. However, care must be taken when implanting CNT modified electrodes, as the porous structure can be squashed during insertion[76].

CNT modified substrates are also able to stimulate neural activity[77]. Vertically aligned pillars of MWNTs were grown on an MEA before growth of hippocampal neurons[78]. The neurons were electrically stimulated, with action potentials monitored by calcium imaging. A random mat of SWNTs was used to interface with hippocampal neurons, electrical stimulation through the mat was monitored by patch clamping of the neurons[79]. A LBL film of PAA and SWNT was formed on ITO with successful stimulation of NG108-15 cells detected by patch clamping[80]. PEDOT-CNT modified electrodes were able to stimulate retinal ganglion neurons, requiring a lower voltage and less charge than TiN electrodes[81]. A CNT fiber was insulated with polystyrene-polybutadiene copolymer, leaving the tip exposed, the fiber was able to stimulate and record neural activity[82].

2.2.4. Carbon Nanotube Composites

Inclusion of CNTs into organic conductor composites can enhance their electrical and mechanical properties. Examples of CNT composites are detailed previously and in sections 2.3, 4 and 5.

2.3. Conducting Polymers

Heeger, MacDiarmid and Shirakawa discovered conducting polymers and were awarded the 2000 Nobel Prize in Chemistry. Conducting polymers (CPs) contain a conjugated backbone. The high conductivity of the polymer usually arises by oxidation of the backbone and incorporation of a charged dopant counter ion. Reduction of the backbone with incorporation of a cation dopant ion and self-doping CPs are also possible[83], but these have rarely been used for neural interfacing.

2.3.1. Synthesis of Conducting Polymers

CPs can be synthesised by several methods that usually involve oxidative coupling. This can be achieved by a chemical oxidant or application of an electric current in solution[83]. Vapor phase polymerisation can also be performed. While the monomers are reasonably soluble in most common solvents, the polymers are not. As a result, during polymerisation, the polymer precipitates from solution, to form a stabilised dispersion or onto a substrate. Vapor phase polymerisation can also be used to pattern substrates. In contrast, during electrochemical polymerisation, the CP forms in close

proximity to the electrode. When the solubility limit of the polymer is reached, the CP precipitates out, and can adsorb onto the electrode surface. Further growth of the CP out from the electrode surface can then occur. The structure and conductivity of the CP is therefore highly dependent on the polymerisation method used. The large variety of monomers, dopant ions and polymerisation methods provides a rich assortment of material properties including hardness, surface charge, charge injection capacity, topography, conductivity and chemical functionality that can control neural growth, structure, differentiation and function[84].

2.3.2. Interfacing Conducting Polymers with Cells

Early work on neural interface development was targeted at reducing the immune response of implanted electrodes, which included CP modified electrodes[85]. One of the first reviews focussing on CP use in medical devices was published in 2007[86]. It encompassed electrical sensing and stimulation, actuators, drug delivery, microfluidics and biocompatibility. Several reviews on CPs used for neural interfaces have been published since[10, 12, 87].

There are reports of CPs as substrates for many different cell types, including PC12s[88-94], rat glial cells[95], astrocytes[96], human neuroblastomas[97, 98], NCTC 2544 keratinocytes[99], primary rat cortical neurons[68, 100-104], rat spinal ganglion neurons[105, 106], primary rat motor neurons[107], rat retina[81], primary rat Schwann cells[108], chick cardiomyocytes[109], primary myoblasts[63, 110], DRGs[111], primary rat NSCs and embryonic stem cell derived NSCs[112], HeLa cells[113], NIH 3T3 fibroblasts[42, 114], L929 fibroblasts[115], human adipose stem cells[116], cardiac and endothelial progenitor cells[117].

There are several different classes of CP, examples of each of these interfacing with cells are given. Polyaniline (PANI) was used for growing cardiac myocytes on its non-conductive emeraldine base (E-PANI) and conductive forms[118]. Initial cell attachment was slightly lower compared to the polystyrene control. Initial cell growth was also slower on the E-PANI compared to PANI and the control. PANI was polymerized with perchloric, hydrochloric, malic, and citric acid dopants or cast onto polytetrafluoroethylene (PTFE)[119]. Stronger acids increased the conductivity of the film with variation in roughness and wettability. PC12 cell attachment was about 70% on the polymerized films, but only 30% on the cast film. There were differences in cell proliferation and morphology on each surface after 4 days culture. The related polymer, *N*-(4-aminophenyl)-*N′*-(4′-(3-triethoxysilyl-propyl-ureido) phenyl-1,4-quinonenediimine) (ATQD), has also been synthesised[120]. PC12s attached to ATQD, but modification of the surface with an RGD peptide improved adhesion, cell proliferation and neurite length.

The majority of publications on CPs for neural interfacing involve PPy. Optically transparent thin films of PPy doped with *p*-toluenesulfonate (pTs) were first reported as a substrate for bovine aortic epithelial cells[121]. Cell attachment was poor on the PPy-pTs films. Coating the oxidized PPy-pTs film with fibronectin allowed cell attachment and spread. The neutral PPy-pTs coated with fibronectin showed cell attachment but they remained round. Formation of PPy-pTs by applying a high potential (overoxidation) reduced the film conductivity and had some effect on attached cell morphology[99].

Changes to the CP dopant and film structure can impact cell behavior. For instance, PPy doped with Cl^-, ClO_4^-, pTs, hyaluronic acid (HA), dextran sulfate (DS), chondroitin sulfate (CS) or poly(2-methoxyaniline-5-sulfonic acid) (PMAS) had different surface morphology, surface roughness, contact angle and Young's modulus[122]. The higher surface roughness appeared to reduce the viability and density of cardiac and endothelial progenitor cells[117]. A similar result was found for primary myoblasts[110]. NSCs were grown on PPy doped with dodecylbenzenesulfonate (DBS), pTs, Cl^- or ClO_4^- and pre-coated with poly L-ornithine and fibronectin[112]. Film roughness was lowest on PPy-DBS, which also had the highest cell viability. NSCs on PPy-DBS were then able to differentiate into astrocytes, neurons and oligodendrocytes in a comparable pattern to cells grown on standard tissue plates. Reduction of the PPy-DBS film resulted in poor viability of the cells and detachment from the CP.

More recently, PEDOT has been recommended for neural interfacing as it is more chemically stable than PPy. Laminin peptide doped PEDOT had a lower surface roughness and hardness than PEDOT-

pTs; they had a lower PC12 cell density but with a larger neurite length[91, 123]. Nerve growth factor (NGF) can also be incorporated into CPs; PPy and PEDOT doped with PSS and NGF enabled growth of PC12 cells[89]. PEDOT doped with pTs or laminin peptide was also grown with entrapped NGF, PC12s were able to grow on the CP, but the neurite length was shorter than cells grown in media with NGF[92]. PEDOT doped with PSS-co-(maleic acid) was unable to grow primary neurons, but after modification with PLL, L1 or N-Cadherin cell adhesion proteins, neurons were viable[104]. L1 modified PEDOT-PSS-co-MA enhanced axonal growth while NCad promoted axonal and dendritic growth. PPy and PEDOT were grown on poly(L-lactic acid) (PLLA) fibers before dissolving the PLLA to form PPy and PEDOT nanotubes[111]. The CP nanotubes induced longer neurite growth than on films of the same composition.

2.3.3. Electrical Stimulation and Recording with Conducting Polymers

The inherent conductivity of CPs allows electrical stimulation of the electrode-neural interface. PC12s grown on PPy subject to electrical stimulation had an increase in fibronectin adsorption[90] and in neurite length compared to non-stimulated cells[88].

CP modified electrodes have been used in vivo for interfacing with neural tissue. NeuroNexus probes coated in PPy-PSS had an increase in surface roughness and decrease in impedance from 10-10^6 Hz with increased deposition time[124]. Acute multi-unit activity was detected during acute implantation in a guinea pig cerebellum. A similar response from guinea pig cerebellum was seen with PPy doped with a silk like polymer[97]. Electrodes coated with PPy doped with DCDPGYIGSR peptide were implanted in guinea pig cerebellum for 3 weeks[125]. The impedance at 1 kHz increased over time but after 2 weeks, 62.5% of the electrodes still recorded neural activity. However there was no correlation between impedance and recording quality. Histology indicated no difference in foreign body response of coated and uncoated electrodes, although coated electrodes did have a higher level of neurofilaments, indicating greater neurite adhesion. PEDOT-PSS was deposited on NeuroNexus electrodes and dip coated with an alginate hydrogel to reduce the electrode surface stiffness[126]. The electrodes were implanted into the auditory cortex of guinea pigs to detect driven activity by playing noise bursts. The signal-to-noise ratio (SNR) decreased with increasing hydrogel thickness, as the neurons were pushed further away from the electrode site. Electrodes coated in a surfactant templated deposition of PEDOT-ClO_4^- were implanted in rat motor cortex for 6 weeks[127]. The impedance increased rapidly from day 3 to 15. The SNR decreased after implantation, on average, 70% of sites provided a SNR greater than 2. Similar results were seen with electrodes coated in PEDOT-ClO_4^- nanotubes templated from PLLA fibers implanted in rat barrel cortex for 7 weeks[128]. PEDOT-PSS coated microwires implanted in a rat somatosensory cortex were able to record neural activity for 1 week[129]. And PEDOT-PSS coated micro-carbon fibers could record activity from rat motor cortex[130]. PEDOT-pTs modified electrodes were implanted into a cat suprachoroidal space[131], the charge injection limit of the modified electrodes was greater than bare platinum electrodes. Neural stimulation at 100 μA resulted in a voltage excursion of 1.5 ± 0.2 V versus 3.3 ± 0.6 V for modified and unmodified electrodes. And the electrodes could induce neural activity, detected by an electrode implanted in the visual cortex.

CP modified NeuroNexus probes were used to understand the relationship between electrochemical behavior and neural recording (Figure 4). Electrodes were modified with PEDOT or PPy doped with pTs or SO_4^{2-} at different deposition times[132, 133]. The charge density was assessed by cyclic voltammetry, varying with CP and increasing with deposition time. The impedance at 1 kHz decreased in the order PPy-pTs>uncoated>PPy-SO_4>PEDOT-SO_4>PEDOT-pTs and a 45 s deposition of PEDOT-pTs was lower than other deposition times. The electrode was placed into a rat inferior colliculus (IC) to record multi-unit activity induced by white noise bursts played through the ear bar. After recording the neural activity, the electrodes were driven further into the IC so that an electrode was positioned in the same spot as the more distal electrode and the neural activity rerecorded. The electrophyiological response was then averaged over multiple recording positions within the IC to remove any biological noise. Correlations of recorded RMS outside the noise stimulation, SNR and mean spike count with impedance at 1 kHz were seen across different CPs but not with varying PEDOT-pTs thickness. The charge density and impedance were also affected by

protein fouling during the acute implantation, with PEDOT-pTs being the most biostable. Follow-up studies measured the effective electrode area and charge density of CP modified electrodes using the reduction of a soluble redox species[134]. A geometric, steady state diffusion or linear diffusion electrode area could be obtained with the charge density dependant on measurement technique. The charge density was also a function of electrode area, limiting the utility of reporting a single charge density value for a material and offers the possibility of increasing charge density of neural electrodes by altering their geometry. Furthermore, the impedance of electrodes for neural interfacing is normally reported at 1 kHz, however an action potential contains information over a much wider frequency range[135]. The impedance at low frequencies was found to more strongly correlate with electrode area, which may be a better estimate of the thermal noise and SNR[136].

Conformal electrodes have been developed for interfacing with the surface of the brain. Gold electrodes on a parylene C substrate were coated with PEDOT-PSS and placed on rat somatosensory cortex to detect neural activity[137]. PEDOT-PSS modified electrodes on a polyimide substrate were placed in a rat cochlear nucleus and able to induce electrically evoked auditory brainstem responses (eABRs)[138].

Recently, a fully organic retinal prosthesis was developed (Figure 5)[139]. The three layer structure comprised a silk fibroin substrate coated with PEDOT-PSS and poly (3-hexylthiophene) (P3HT). When attached to the retina of dystrophic RSC rats (a model of retinitis pigmentosa), electrophysiological and behavioral analyses indicated recovery of visual acuity for up to 10 months after surgery. However the mechanism of neural stimulation is not clear at present.

CPs could also be polymerized directly onto neural tissue. PEDOT-PSS was grown on neuroblastoma derived cells or mouse cortical cells[140]. Enzymatic and mechanical disruption was used to remove the cells, leaving a porous neural template. Although reseeded cells on the porous structure preferentially grew on un-templated regions. It was then demonstrated that PEDOT-PSS could be deposited onto brain slices[141] and grown in vivo[142] to create an electrode that integrates with neural tissue for better electrophysiological performance. However a foreign body response was elicited around the entire CP region.

Organic electrochemical transistors (OECT) have been formed from PEDOT-PSS for neural interfacing. A flexible parylene substrate was patterned with gold electrodes and spin coated with PEDOT-PSS[143]. The ECoG was placed on the surface of a rat cortex. Application of a potential to the gate electrode changed the doping of the PEDOT and its transconductance. The OECT was then able to measure lower level neural activity compared to a normal electrode. The OECT has also been used to record EEG, EOG and ECG[144]. The OECT could then be used to stimulate neural activity too[145].

2.3.4. Conducting Polymer Composites

Further modification of CPs for neural interfacing can be achieved by creation of composites. Graphene-based materials[41, 42] and CNTs[63, 71, 103, 146] have been used with CPs, combining the electrical and mechanical properties of the graphene and CNTs with the chemical functionality of the CPs. PEDOT doped with Keggin type polyoxometalates displayed multiple Faradaic processes, significantly increasing the charge injection capacity of the electrode[147]. PEDOT doped with the ionic liquid 1-ethyl-3-methylimidazolium bis(trifluoromethylsulfonyl) imide (EMIIM) had a very porous structure with a lower impedance at 1 kHz than PEDOT-PSS and was able to record activity from a rat barrel cortex[148]. Different metal nanoparticles have been incorporated into PEDOT, modifying the film morphology[149]. Poly(ethyleneglycol) (PEG) is routinely used in medical applications and has low cell adhesion properties, PEDOT-pTs mixed with PEG had a high conductivity and good cell adhesion[113].

There is a mechanical mismatch between the soft neural tissue and the stiff electrode and its coatings, leading to poor chronic biocompatibility of implanted devices. Hydrogels are soft, flexible materials with a high water content making them very similar to neural tissue. There are several reports of CPs mixed with hydrogels to form soft, conductive interfaces[150]. PPy-gellan gum was electrodeposited to form a highly porous conductive network[151]. It had an impedance at 1 kHz of only 44 Ω and a large

charge injection capacity. PEDOT was deposited on polyurethane and hydrogel scaffolds to create flexible electrodes that could be stretched up to 100% without fracture[152]. The conductivity of the film was stable with up to 50% elongation. And NG108-15 and C2C12 cells were viable on the structure. Hydrogels formed from methacrylated gelatin, sericine, heparin and poly(vinyl alcohol) (PVA) were soaked in EDOT and pTs before polymerisation to form PEDOT-pTs hydrogel hybrids that were able to support PC12 growth[153]. PEDOT was copolymerized with acrylic acid in the presence of poly(ethylene glycol) diacrylate, the hydrogel could swell up to ~5000% in water[154]. C2C12s were able to grow on the substrate and penetrated up to ~2 mm into the swollen hydrogel. PEDOT has also been grown in alginate, the conductive hydrogel was implanted into rat peroneal nerve gaps to promote axonal growth[155].

3. Neurotransmitter Detection and Drug Elution

As well as facilitating direct electrical communication with living cells, implantable electrodes may provide information on cell function through monitoring of neurotransmitters –providing more specific details on cell behavior and disease states. For instance Parkinson's disease is associated with a decrease in dopamine in the brain. A further dimension may involve building chemical communication systems (such as ionic, drugs or growth factors) into the electrode structure.

As well as electrical recording, graphene-based materials are capable of measuring neurotransmitters. For instance, a carbon fiber was immersed in a rGO dispersion for 5 minutes and then rinsed in water. The modified fiber was placed near mouse hippocampus slices and dopamine was detected by cyclic voltammetry[156].

Carbon fibers are routinely used for the detection of neurotransmitters[157], however the fibers are fragile, and can be easily broken during use. A number of reports have been made of CNT fibers recording various neurotransmitters and analytes[158] including dopamine[159], NADH and glucose[160]. The surface functionality allows CNT electrodes to record action potentials and measure dopamine[161]. CNT fibers are not only more flexible and robust compared to carbon fibers, CNT fibers are also more resistant to dopamine fouling, resulting in longer electrode lifetimes[162].

CPs are capable of detecting neurotransmitters with chromaffin cells placed on PEDOT-PSS modified electrodes, exocytotic processes were achieved by gently pressing the cell with a glass pipette. Holding the potential at 700 mV vs Ag/AgCl, amperometric spikes detected release of catecholamines[163]. PPy-PBS was overoxidised by applying a potential of 989 mV for >40 minutes and coated with Nafion for dopamine detection or Nafion and then glutamate oxidase for glutamate detection[164]. Highly selective measurements of dopamine and glutamate could then be achieved by amperometry. PEDOT, poly(N-methylpyrrole) (PNMPy), poly(N-cyanoethylpyrrole) (PNCPy) and poly(hydroxymethyl-3,4-ethylenedioxythiophene) (PHMeDOT) doped with ClO_4^- were used to detect dopamine, adsorption of gold nanoparticles onto the surface of the CPs increased the electron transfer rate and sensitivity[165].

Drug elution can be achieved with graphene-based materials. Nano-GO was modified with polyethylene glycol (PEG) to increase its solubility[166]. This modified nano-GO could then adsorb doxorubicin, a widely used cancer drug. Lowering the pH from 8 to 5.5 then released the drug into cell culture. In another example, nano-GO was sulfonated and then modified with folic acid before adsorption of doxorubicin and camptothecin, another anti-cancer drug[167].

The polymerization process of CPs allows the entrapment of pharmacological agents. Several articles report inclusion of dexamethasone (Dex) as a dopant anion[74, 101, 168]. Dex is a steroid, which can reduce inflammation associated with electrode implantation. Application of a negative potential reduces the CP and the Dex is eluted, reducing inflammation for an acute period after surgery. Co-doping of Dex with valproic acid, an anticonvalescent was also demonstrated[169]. The nerve growth factor NT3 has been included in CP modified electrodes to enhance neural growth to the electrode surface[106]. The NT3 can passively diffuse out of the CP, but electrical stimulation enhanced NT3 release, with neurite growth correlated with amount of NT3 released[105]. Cochlear implants modified with PEDOT-pTs with or without NT3 entrapment were implanted in guinea pigs for 2 weeks[170]. Animals with NT3 had higher spiral ganglion neuron (SGN) survival rate and lower eABR thresholds

than without NT3. Overoxidised PEDOT soaked in GABA, glutamate or aspartate could release the neurotransmitters when electrically stimulated and induce a neural response[96]. And use of inhibitors of NMDA and AMPA-type glutamate receptors, 2-amino-5-phosphonopentanoate (AP5) or 6-cyano-7-nitroquinoxaline-2,3-dione (CNQX) as dopants in PPy, could block neural activity when PPy was reduced[102].

4. Advances in Fabrication

Initial electrodes for interfacing with neurons were fabricated from metal wires[171]. The wire could be drawn to the desired diameter, dip coated in an insulating material to shield the edges, mechanically polished, cut or etched to form a sharp tip, and soldered to an external connector for electrical contact. Arrays of wires could be built for recording and stimulating from multiple neurons[172], but implanting each of the wires was complex, giving poor reproducibility. Glass pipettes were also used to patch directly onto cells, with the development of the gigaseal and patch clamping being awarded the Nobel prize in Physiology or Medicine in 1991[173]. However glass pipettes are extremely fragile and not suitable for chronic implantation or human use. Development of silicon microfabrication allowed reproducible production of electrode arrays[174]. Improvements in design has enabled 2D and 3D electrode arrays for interfacing with larger neural populations[175]. These silicon electrode arrays are fragile and stiff, and when implanted into the body, an immune response encapsulates the electrode, compromising performance[176]. Electrode arrays have been lithographically patterned onto silk[177] or polymer films to allow the electrodes to be placed on the surface of the brain[178], peripheral nerves[179] or around the heart[180]. Recently, syringe injectable electronics have been developed; these flexible, minimally invasive electrodes have been able to stimulate and record activity from neurons (Figure 6)[181, 182]. Another recent approach for reducing surgical trauma involves inserting a stent electrode array into a cerebral vein (Figure 7), which doesn't require disruption of the blood-brain barrier. Electrodes on the stent can then record from the motor cortex near the vein[183, 184].

The limitation of the current electrodes includes fragility and high stiffness with no cues for controlling neural growth or integration into the electrode; leading to poor cytocompatibility and low biostability. Current electrode constructs used for cortical implants do not provide chronic stability. Electrodes used to record neural behavior show a change in response over time due to neural rearrangement, protein fouling and encapsulation from scar tissue. Modification of electrodes with organic conductors has met with limited success, as the electrode surface is only a small part of the total device footprint and the rigid electrode design maps poorly onto the complex 3D neural structure. The development of new fabrication techniques allows the formation of novel electrode systems for neural tissue interfacing. New electrode systems can incorporate different mechanical, physical and chemical cues for guiding neural growth to the electrode and tailor the device for specific applications. Below we review other advances in fabrication that can be used to produce organic electrode materials in forms of relevance to neuronal communications. Although in most cases the combination of organic conducting materials and neural tissue has yet to be fully exploited.

4.1. Fiber Spinning

4.1.1. Wet Spinning

Wet spinning involves injecting a feed solution containing the constituents of interest into a coagulation bath (Figure 8). As the feed solution precipitates, it is drawn out into a fiber. The fiber can then be passed through other washing baths and collected on a spool. Variation in the injection rate and nozzle diameter can control the fiber diameter. The feed and coagulation bath constituents can be used to create one-component or composite fibers. A number of publications have demonstrated wet spinning of graphene-based materials[185, 186], CNTs[187] and CPs including PANI[188], PEDOT[189] and PPy[190]. Some materials are poorly soluble, limiting their concentration in the feed solution. GO can be dispersed in the feed solution and after fiber spinning, treated to form rGO fibers (Figure 9)[185, 186]. The drawing of 1 dimensional fibers then orientates the components, leading to an increased conductivity and strength compared to non-aligned materials. Biomolecules such as chitosan, DNA, hyaluronic acid, heparin and chondroitin sulfate can be included in the feed solution to stabilize the dispersion before spinning, and creation of composite fibers[191], the biomolecules can

also be placed into the coagulation bath to create core-shell fibers[192]. An alternative approach involves reactive wet spinning, for example, pyrrole monomer is dissolved in the feed solution and polymerized in the coagulation bath[193].

Wet spun fibers have been used as a substrate for cell culture. 75:25 PLA/PLGA was wet spun into 30 μm diameter fibers onto gold coated mylar[194]. PPy-pTs was then electrodeposited in between the fibers and the whole scaffold coated in poly (L-ornithine) and laminin. DRGs were then cultured on the scaffold and a biphasic electrical stimulation protocol of charge-balanced pulses of 100 ms pulse width, 3.78 ms interphase gap and 0.2 ms short circuit at 250 Hz applied for four days for 8 h per day. A significant increase in axonal growth was achieved with the electrical stimulation. The axon growth was directed by the biodegradable hydrogel fibers. DRGs grown on plain PPy-pTs showed unguided, radial growth of axons. Myoblasts were also cultured on the scaffolds with the majority of myotubes orienting less than 10° from the fiber axis, while myotubes were unoriented in the absence of the fibers[195]. An interfiber distance of 160 μm or less produced the highest myotube alignment, increasing interfiber distance reducing the myotube alignment.

A dispersion of PEDOT-PSS in water was injected into a coagulation bath containing chitosan and washed with ethanol[196]. The fiber was then treated with ethylene glycol and heated to 120° for 30 min to increase the conductivity. The fiber was subsequently placed into a solution containing pyrrole and the antibiotic ciprofloxacin hydrochloride. Using the PEDOT-PSS fiber as an electrode, PPy doped with ciprofloxacin was electrodeposited, creating a core-shell structure. Electrical stimulation of the fiber enabled release of the ciprofloxacin to create zones of inhibition against E. coli and S. pyogenes. B35 neuroblastomas were able to proliferate on the fibers, indicating they weren't cytotoxic.

4.1.2. Electrospinning

Electrospinning is an approach to fiber formation that enables dimensions in the nanometer domain to be attained. The organic conductors are dispersed in a feed solution in a spinneret. A high voltage is applied to the spinneret above a grounded conductive collecting target. The voltage on the spinneret charges the feed solution until electrostatic repulsion overcomes the surface tension of the droplet at the spinneret tip. At a critical potential, the droplet erupts in a Taylor cone. If the solution is sufficiently cohesive, a charged jet is formed, otherwise droplets are ejected. The charged jet dries during flight and the charges migrate to the jet surface. Electrostatic repulsion induces a whipping motion of the jet, resulting in fiber thinning and elongation. The fiber then deposits on the grounded target as a tangled mat. By collecting the fiber on a rotating bobbin, an aligned fiber can be obtained[197]. Electrospinning with pure dispersions of organic conducting materials is difficult, so inclusion of a spinnable polymer such as polyethylene oxide or polystyrene facilitates the process [198]. However these polymer blends compromise conductivity to afford appropriate mechanical properties. A comprehensive review on electrospinning including different materials used to form fibers is available[199].

In one publication, PLLA fibers were spun from different concentration feed solutions[200]. Fiber diameters ranged from around 150 nm to 3000 nm with increasing polymer concentration. Aligned fibers had a smaller diameter compared to random mats due to the high rotation speed of the collection bobbin stretching the fiber. NSCs cultured on the aligned fibers showed highly oriented outgrowth.

Electrospun poly(ε-caprolactone) (PCL) or PLA was dipped into a pyrrole solution with chemical oxidant to form a PPy sheath[201]. The PPy uniformity was affected by the CP dopant and the wettability of the electrospun fiber. Soaking in dichloromethane for 24 hours could dissolve the core, leaving PPy nanotubes. DRGs cultured on the aligned hollow or core-shell fibers displayed directed growth, and electrical stimulation increased neurite length.

Vapor phase polymerisation of PEDOT-pTs on electrospun poly(ethylene terephthalate) (PET) coated with chemical oxidant produces a more uniform sheath, the core-sheath fiber was able to support SH-SY5Y human neuroblastoma growth[202].

PANI doped with camphorsulfonic acid was blended with poly(L-lactide-co-ε-caprolactone) (PLCL) and electrospun into fibers[203]. Both NIH-3T3 fibroblasts and C2C12 cells proliferated well on the fibers.

CNTs dispersed in solution with a polymer can be electrospun, producing aligned CNTs within the composite fiber[204]. SWNTs dispersed with poly(styrene-*β*-isobutylene-*β*-styrene) (SIBS) were electrospun into random mats and supported L292 fibroblast proliferation[205]. Graphene-based materials can also be incorporated into electrospun fibers. For instance, an electrospun poly(vinyl chloride) (PVC) fiber was NH_3 plasma treated before coating with GO which was then chemically reduced to rGO[206]. Primary motor neurons extended neurites along the rGO coated fibers with electrical stimulation increasing the neurite length.

4.1.3. Carbon Nanotube Drawing

Pure fibers of aligned CNTs can be formed by drawing strands from a CNT forest[207]. Draw was initiated by application of an adhesive strip to the side of a MWNT forest and slowly hand drawing. The aerogel sheet thickness increased with longer MWNT length. The sheet could then be compressed by dipping it in liquid. Spinning the drawn sheet can be used to obtain CNT fibers[208]. The high strength of the fibers allows knitting, knotting and braiding to obtain complex structures. Primary myoblasts could be grown on MWNT sheets[63]. Coating the MWNT sheet with PPy-pTs improved the cell viability, but thick PPy-pTs coatings reduced the alignment of the myotubes to the underlying MWNTs.

4.2. Printing

4.2.1. Inkjet Printing

The ability to create stable dispersions of organic conducting materials enables their use as inks in different printing processes. Inkjet printing transfers droplets of ink from a printhead onto a substrate to form 2D patterns over large areas. Commercial printers are extremely cheap and easily modified to handle novel ink formulations. Multiple printheads also allow different inks to be used on the one image. Ink can be printed in a continuous stream or by drop-on-demand. Drop-on-demand is achieved by thermal (bubble jet) or piezo printing. In thermal printing, heat is applied to the nozzle and solvent vaporisation causes a droplet to be ejected. This usually requires the solvent to be aqueous, which limits the types of printable materials. Piezo printing uses a small piezoelectric crystal in the printhead, application of a voltage modifies the piezoelectric crystal shape which forces a droplet out of the nozzle. For both printer types, droplet volumes of ~10-20 pL are produced, generating droplet diameters ~30-40 μm.

Optimisation of an ink for inkjet printing involves modification of ink viscosity and surface tension and ensuring the ink dispersion is stable over the entire print run. There have been reports of inkjet printing of PANI[209], PPy[210] and PEDOT[211]. In an alternative method, a chemical oxidant can be printed and the image exposed to vapor phase polymerization[212]. It is also possible to disperse CNTs[213] and graphene-based materials[214] in inks for inkjet printing. These patterned substrates can then be used to control cell growth[215].

4.2.2. Extrusion Printing

Structures can be printed by extrusion printing, where a gel or molten material is forced out of a nozzle onto a substrate. The continuous polymer matrix formed by extrusion ensures higher conductivity than inkjet printing of individual droplets. Multiple layers can also be extruded of one or more different inks to build up 3 dimensional scaffolds. A concentrated dispersion of PEDOT-PSS was extruded onto glass or a chitosan-hyaluronic acid hydrogel[216]. The line width was 522 μm on glass and 180 μm on the hydrogel. PEDOT-PSS tracks could also be extruded into the hydrogel. PEDOT doped with dextran sulfate (DS) was dispersed at ~10% in water and extruded onto a glass slide with an average line width of 265 μm[115]. PEDOT-DS could also be spray coated or inkjet printed. L929 fibroblasts were then able to proliferate on the printed substrates.

MWNTs were dispersed in gellan gum; increasing concentration of MWNT or gellan gum increased the dispersion viscosity to enable extrusion printing[217]. Higher MWNT mass fraction also increased

the dispersion conductivity. Tracks were extruded on a variety of substrates. Tracks printed on a flexible substrate could be stretched, increasing their resistivity, acting as a strain gauge.

Powdered graphene dispersed with polyester polylactide-co-glycolide, a surfactant and plasticizer in dichloromethane (DCM) could be extruded with the DCM evaporating after printing[218]. hMSCs proliferated well on the scaffolds. The scaffolds were also implanted subcutaneously for 30 days in mice and did not elicit an inflammatory response or fibrous encapsulation. Aqueous dispersions of GO can be extruded[219] and subsequently reduced to rGO[220]. An rGO-chitosan dispersion was extruded into 30 layer, 1.5 cm^2, 3D scaffolds with a 500 μm^2 pore size[221]. L929 fibroblasts adhered and proliferated through the entire 30 layers of the scaffold.

5. Cytotoxicity of Organic Conductors

Any material proposed for a biomedical application must be biocompatible. This can be assessed in culture on large samples by cell growth and proliferation, measurement of metabolic activity and necrosis. In vivo behavior of the material must be tested as the immune response is more complex. Use of new fabrication methods may result in different material geometries (eg. nanofibers and nanoparticles), which can affect the immune response. After implantation, degradation of the materials can also result in movement of small particles far from the initial implantation site. As such, a general understanding of the potential cytotoxicity of organic conductors of varying composition and geometry is required.

To assess the cytotoxicity of carbon-based materials, PC12 cells were cultured with graphene and SWNTs[29]. Graphene and SWNTs were purified by washing with hydrochloric acid and then dispersed in 2-propanol under sonication. PC12 cells were grown in 96 well plates for 48 hours before adding varying amounts of graphene or SWNT (0-100 μg/mL) for 24 hours. The zeta potential of the two materials indicated purity above 98.5%, however the zeta potential changed to the same value on both materials after dispersion in culture medium, indicating protein binding affects the surface charge. An MTT assay was used to assess metabolic activity after addition of the carbon-based materials. After 24 hours, the metabolic activity of the cells decreased in a concentration dependant manner. Graphene was more cytotoxic then SWNTs at low concentrations, while SWNTs were more cytotoxic at higher concentrations. Membrane damage and necrosis was assessed by measuring lactate dehydrogenase (LDH). SWNTs induced a large increase in LDH, while graphene only impacted the LDH at 100 μg/mL. Formation of reactive oxygen species (ROS) was concentration and time dependant, indicating oxidative stress was occurring, although caspase 3 activation was low, so that the apoptosis pathway was weak. Therefore graphene and SWNTs have concentration dependant cytotoxicity, but particle shape and agglomeration may play a role.

The cytotoxicity of GO was investigated in comparison to SWNTs and MWNTs[222]. GO was prepared by Hummers' method, washed in hydrochloric acid then milli-Q water, suspended in water and dialysed to remove residual metal ions and acid. Some GO was incubated with fetal bovine serum (FBS) or bovine serum albumin (BSA). There was a strong adsorption of FBS protein and BSA to the GO, more than occurred on SWNTs and MWNTs. A549 cells were cultured in 24 well plates before addition of the carbon-based materials (0-100 μg/mL) for 24 hours. An MTT assay showed an increase in cytotoxicity with increased GO concentration, and a slightly higher toxicity compared to the CNTs but no time dependence, whereas MWNTs have been previously shown to have a time dependant cytotoxicity[223]. Transmission electron microscopy of the cells revealed the GO had severed the cell membrane, leading to leakage of cytoplasm and inducing cell death. Coating the GO with FBS protein or BSA did not reveal any cytotoxic effects. This work demonstrates direct interaction between GO and the cell membrane leads to cell death, and not oxidative stress. And the impact of GO-neural interaction can be mitigated by treatment with an appropriate peptide.

Classification of CNTs as biocompatible or non-biocompatible is not possible, the CNT structure, dose, administration site and functionalization can all play a role[11, 224] and bioaccumulation can occur in organs far from the initial exposure site[225]. The cytotoxicity of CNTs has been assessed by several groups[51, 77]. CNTs, carbon nanofibers and carbon nanoparticles were suspended in gelatin solutions and exposed to different human lung tumour cell lines, the cells displayed a dose dependent

toxicity[223]. Mouse fibroblasts showed changes in metabolic activity, reduced viability and cell death with increasing CNT concentration; impurities in the CNTs increased their toxicity [226]. Comparison of CNT toxicity with graphene-based materials on fibroblasts[26] and PC12s[32] indicated cells were less viable and with fewer neurites on CNTs. An MTT assay demonstrated lower mitochondrial activity and higher level of cell membrane damage on SWNTs than on graphene[29]. Exposure of a whole organism to fullerenes was performed on fish, which resulted in an increase in lipid oxidation in the brain, indicating activation of a ROS pathway[227]. PPy-SWNTs were deposited on platinum electrodes and implanted into rat brain for 6 weeks, the immune response to modified and unmodified electrodes was very similar, indicating good biocompatibility[93]. MWNT modified electrodes implanted into rat hippocampus displayed no increase in inflammation compared to controls[228].

The large variety of CPs prevents labelling them all as biocompatible or non-biocompatible[229]. An MTT assay showed higher PC12 survival rate on PANI than a silicon substrate[230]. Keratinocytes were successfully grown on PANI and PPy, while subcutaneous implantation in a rat for 4 weeks generated a fibrous capsule but no necrosis or degeneration around the implant[231]. There was also minimal inflammation after 50 weeks subcutaneous implantation[232]. Skin irritation tests of PANI were classed as non-irritating; cytotoxicity was concentration dependant, being considered fairly high, although purification by reprotonation and deprotonation significantly reduced the cytotoxicity[233]. The high cytotoxicity was attributed to residual low-molecular weight products such as hydrochloric acid after polymerisation.

Cytotoxicity testing was undertaken on PPy powder chemically polymerized by ferric chloride and films electrochemically polymerized with chloride dopant on ITO[234]. Acute testing by injecting the powder into mice abdominal cavity gave no adverse response for up to 30 days. Pyretogenesis tests by intravenous injection of the powder into rabbits resulted in minimal change in body temperature. An MTT assay on Schwann cells was deemed non-toxic. There was no evidence of hemolysis when mixed with blood samples from rabbits, nor an allergic response when injected into guinea pigs for 14 days. Peripheral nerve tissue grown on PPy films had more and longer neurite growth compared to bare glass substrates after 3 weeks. Implantation of a PPy-silicon tube for 6 months in rat peripheral nerve displayed only minor inflammation. PPy nanoparticles have also been assessed on different cell types, the cell morphology and viability was affected by PPy nanoparticles with a dose dependence[235]. The cytotoxicity of CP coated silica nanoparticles also displayed dose dependent response with PPy giving the highest viability and PT the lowest, PEDOT and PANI being intermediate[236]. A nanocellulose-PPy composite was deemed non-cytotoxic[237]. The biocompatibility of a modified PPy has also been assessed, poly(*N*-methylpyrrole) doped with ClO_4^- had good cell attachment and viability[238].

The cytotoxicity of PEDOT-PSS and PEDOT-PBS was assessed with mouse myocytes and deemed biocompatible[239]. PEDOT doped with PSS, heparin, fibrinogen or hyaluronic acid was also found to be non-cytotoxic in cell culture, and platinum foil coated with PEDOT placed into neural tissue for 6 weeks had no difference in immune response compared to control implants[240]. Another study showed PEDOT-PSS, poly (3-hexylthiophene) (P3HT), poly(2-methoxy-,-5-(2′-ethyl-hexyloxy)-p-phenylenevinylene) (MEH-PPV) and poly(9,9-dioctylfluorene-alt-bithiophene) (F8T2) were all non-cytotoxic[241].

6. Conclusions and Future Outlook

Interfacing electrodes with neurons has provided crucial information on neural behavior in normal and pathological conditions. Implanted electrodes can be used to control prosthetic devices or stimulate neurons to mitigate chronic pain, tremor and dyskinesia associated with Parkinson's disease or provide sensory cues for profoundly deaf or blind people. Microelectrode arrays are also able to interface with cell culture and tissue slices. While significant results have been achieved with metal electrodes or glass pipettes, these electrode constructs have limited biocompatibility and biostability, leading to electrode encapsulation, increasing power usage, reducing signal-to-noise ratio and eventual device failure.

Modification of electrodes aims to reduce impedance and increase charge injection capacity. It also aims to control neural growth and scar tissue encapsulation, leading to improved cytocompatibility

and biostability. An increasingly large variety of organic conducting materials including conducting polymers, carbon nanotubes and graphene-based materials are being developed for electrode-neural interfaces. Changes in material properties, including stiffness, charge, roughness, chemical functionality and contact angle have been shown to control cell viability, growth and differentiation. Most of these materials have also shown minimal cytotoxicity. Many forms of electrode modification have increased charge injection capacity and reduced electrode impedance.

6.1. Material Selection

When choosing a material for interfacing with cells, the specific application must be taken into account. Most of the organic conducting materials have shown minimal cytotoxicity, especially at low dosage levels or when formed into devices. PANI could be cytotoxic if residual acid levels were high, although purification improved this. Graphene and CNTs were also able to disrupt the cell membrane, however these effects generally occurred on initial contact and were concentration dependent. Cell attachment and proliferation has been demonstrated on all classes of organic conducting materials. Initial cell attachment may be low on some materials, but coating the surface with a cell adhesion molecule increases cell count. The redox behavior of CPs enables modification of the surface charge, which can be used to alter cell shape and attachment by simply applying a potential. Changes in CP fabrication method and dopant are able to alter the surface properties including roughness and wettability which also affects cell growth. Therefore, careful choice of material and applied potential can be used to control cell attachment and growth.

Many applications of cell interfacing require electrical stimulation or recording, the material must therefore be highly conductive. Graphene and CNTs are inherently conductive, however poor solubility limits their processability. Introduction of functional groups (eg. forming GO), increases the solubility of these materials, but also reduces their conductivity. Subsequent removal of the functionality (eg. formation of rGO) increases the conductivity, but is unlikely to produce properties equivalent to pristine graphene or CNT. The conductivity of CPs is dependent on fabrication method, type of polymer, redox state and dopant ion. Chronic stimulation of cells with CPs can result in over-oxidation of the polymer and loss of dopant, leading to a reduction in conductivity, degradation of the material and delamination from the underlying substrate. Therefore, use of graphene and CNTs may give better long term stability.

Graphene, CNTs and CPs are all relatively stiff materials compared to tissue. The high strength of CNTs and graphene make them useful materials for high load applications. When used as a substrate for cell culture, the mechanical properties are not highly critical. When these materials are implanted, an immune response results in encapsulation of the device. This can increase the distance from the electrode to the target tissue, reducing recording signal-to-noise ratio and increasing power usage for electrical stimulation. Reducing the material stiffness can help overcome mechanical mismatch between the device and the tissue. There have been multiple reports of organic conducting materials being incorporated into hydrogels[242]. Further work on these soft, flexible and conductive hydrogels will provide more guidance on the best materials for chronic, electrical interfacing with cells. Reducing device size can also help evade an immune response, with thin fibers of conducting materials able to perform chronic electrical interaction with cells. Implantation of thin, flexible fibers has been achieved by stiffening with a soluble support material. Recent reports of injectable electronics and a stent electrode are promising new methods of evading an immune response and offer new opportunities for modification with organic conducting materials.

Combined electrical and optical interrogation of cells is increasingly being required for calcium imaging or optogenetic studies, traditional metal electrodes are opaque and ITO is stiff and fragile. Thin films of each organic conducting material have been fabricated and used for optical and electrical experiments. The recent report of an all organic retinal prosthesis using CPs is a unique application for these materials.

For detecting neurotransmitters, the conducting material must be selective and sensitive to the target compound. This is achieved by introducing functional groups onto the surface of the organic material. Oxidation of graphene and CNTs can increase the selectivity towards dopamine without affecting the bulk material properties. Over-oxidation of CPs can increase its selectivity for detecting

neurotransmitters, but can degrade the material conductivity and mechanical robustness. In contrast, CPs are able to entrap drugs with electrical stimulation capable of controlled release.

6.2. Fabrication Method Selection

The high processability of organic conducting materials enables the use of advanced fabrication techniques. Unlike traditional metal working or glass blowing, organic conducting materials can be dispersed in different matrices. They can then be used in various fiber forming and printing processes to create complex 1-, 2- and 3-dimensional constructs. Composite materials such as conductive hydrogels, core-shell fibers and hollow tubes can also be produced. This enables construction of tailor-made electrodes for interfacing with and controlling neurons.

The target application and choice of materials will define the best fabrication method. For high purity graphene or CNTs (eg. for FETs), CVD is typically used. This can be grown directly onto the substrate or transferred. CPs can also be vapor polymerized to cover large areas. Some substrates are not stable at high temperatures for CVD or have a complex geometry that prevents transfer of preformed material. For more controlled growth of CPs or variations in composition, electrochemical deposition is possible. This generally creates more conductive materials than vapor deposition, but low solubility of the monomer limits film growth rate. Dispersions of GO and functionalised CNTs can be used to modify surfaces with subsequent removal of functionalisation by thermal, chemical or electrochemical methods to increase the material conductivity. For patterned deposition of materials, inkjet printing or dip pen nanolithography (DPN) for higher resolution can be used. These methods don't require a conductive substrate for deposition but are slow to fabricate and require a stable ink. Extrusion printing can produce larger structures, including 3D constructs. The extruded lines are also continuous, ensuring higher conductivity across the material than from discrete droplets formed from inkjet printing or DPN. If fibers, sheets or mats are required, CNTs can be drawn, while graphene and CPs must be wet spun or electrospun. Electrospinning can produce very fine fibers, but the materials must be stable and suitable for the electrospinning process. Inclusion of other polymers into the feed solution can allow some unspinnable materials to be used, but will compromise the fibers conductivity. Wet spinning is a more versatile method for forming fibers and variations in feed and coagulation solutions can create multiple layered structures.

Future developments of organic conducting materials will involve development of more complex composites. This will include modification with biomaterials to control cell behavior. Conducting materials will be formed into soft, flexible and biodegradable matrices forming conducting hydrogels that can be integrated into tissue while controlling the immune response. The composites can then combine electrical, topographic, mechanical and chemical cues for guided cell growth and integration in different tissue. They will also allow electrical recording and stimulation and drug elution to measure and control cell behavior and any immune response over different time scales.

Improvements in advanced fabrication will allow production of more complex 3D scaffolds. Material properties such as increasing stiffness or fiber diameter can be strategically distributed throughout a scaffold. The changing scaffold properties can be used to create layered tissue structures for more realistic and functional tissue models or implants.

Combining advanced fabrication and new materials will allow cells to remain viable while suspended in an ink cartridge. The cells can then be integrated into the fabrication process, eliminating the need to seed them onto prefabricated scaffolds. Ultimately leading to fabrication of electrode constructs directly in tissue via a BioPen[243].

Acknowledgements

Funding from the Australian Research Council CentreCenter of Excellence Scheme (Project Number CE140100012) and the HEARing CRC, established and supported under the Australian Government's Cooperative Research s Program are gratefully acknowledged. GGW is also grateful to the ARC for support under the Australian Laureate Fellowship scheme (FL110100196).

References

[1] *Neurological Disorders: Course and Treatment*, Academic Press, San Diego 2003.

[2] M. J. Cook, T. J. O'Brien, S. F. Berkovic, M. Murphy, A. Morokoff, G. Fabinyi, W. D'Souza, R. Yerra, J. Archer, L. Litewka, S. Hosking, P. Lightfoot, V. Ruedebusch, W. D. Sheffield, D. Snyder, K. Leyde, D. Himes, *Lancet Neurol.* **2013**.

[3] P. Heiduschka, S. Thanos, *Prog. Neurobiol.* **1998**, *55*, 433.

[4] L. J. Garey, W. Y. Ong, T. S. Patel, M. Kanani, A. Davis, A. M. Mortimer, T. R. E. Barnes, S. R. Hirsch, J. Neurol. Neurosurg. Psychiat. **1998**, *65*, 446.

[5] S. T. DeKosky, S. W. Scheff, *Ann. Neurol.* **1990**, *27*, 457.

[6] S. Reardon, *Nature* **2014**, *511*, 18.

[7] M. Gay, *The brain electric : the dramatic high-tech race to merge minds and machines*, Farrar, Straus and Giroux, New York 2015.

[8] G. G. Wallace, S. E. Moulton, G. M. Clark, *Science* **2009**, *324*, 185.

[9] S. H. Ku, M. Lee, C. B. Park, *Adv. Healthcare Mater.* **2013**, *2*, 244.

[10] P. Fattahi, G. Yang, G. Kim, M. R. Abidian, *Adv. Mater.* **2014**, *26*, 1846.

[11] N. A. Kotov, J. O. Winter, I. P. Clements, E. Jan, B. P. Timko, S. Campidelli, S. Pathak, A. Mazzatenta, C. M. Lieber, M. Prato, R. V. Bellamkonda, G. A. Silva, N. W. S. Kam, F. Patolsky, L. Ballerini, *Adv. Mater.* **2009**, *21*, 3970.

[12] M. Asplund, T. Nyberg, O. Inganas, Polymer Chemistry 2010, 1, 1374; R. Green, M. R. Abidian, Advanced Materials 2015, 27, 7620; M. Jorfi, J. L. Skousen, C. Weder, J. R. Capadona, *J. Neural Eng.* **2015**, *12*, 011001.

[13] A. Ambrosi, S. Y. Chee, B. Khezri, R. D. Webster, Z. Sofer, M. Pumera, *Angew. Chem. Int. Ed.* **2012**, *51*, 500.

[14] R. L. McCreery, *Chem. Rev.* **2008**, *108*, 2646.

[15] D. D. L. Chung, *J. Mater. Sci.* **1987**, *22*, 4190.

[16] K. S. Novoselov, A. K. Geim, S. V. Morozov, D. Jiang, Y. Zhang, S. V. Dubonos, I. V. Grigorieva, A. A. Firsov, *Science* **2004**, *306*, 666.

[17] W. Choi, I. Lahiri, R. Seelaboyina, Y. S. Kang, *Crit. Rev. Solid State Mater. Sci.* **2010**, *35*, 52.

[18] D. R. Dreyer, S. Park, C. W. Bielawski, R. S. Ruoff, *Chem. Soc. Rev.* **2010**, *39*, 228.

[19] S. Niyogi, E. Bekyarova, M. E. Itkis, J. L. McWilliams, M. A. Hamon, R. C. Haddon, *J. Am. Chem. Soc.* **2006**, *128*, 7720.

[20] P. Nguyen, V. Berry, *J. Phys. Chem. Lett.* **2012**, *3*, 1024.

[21] L. Yang, Y. Li, Y. Fang, *Adv. Mater.* **2013**, *25*, 3881.

[22] B. C. Thompson, E. Murray, G. G. Wallace, *Adv. Mater.* **2015**, *27*, 7563.

[23] M. Kalbacova, A. Broz, J. Kong, M. Kalbac, *Carbon* **2010**, *48*, 4323.

[24] S. Y. Park, J. Park, S. H. Sim, M. G. Sung, K. S. Kim, B. H. Hong, S. Hong, *Adv. Mater.* **2011**, *23*, H263.

[25] M. Kalbacova, A. Broz, M. Kalbac, *J. Biomed. Mater. Res. Part A* **2012**, *100A*, 3001.

[26] S.-R. Ryoo, Y.-K. Kim, M.-H. Kim, D.-H. Min, *ACS Nano* **2010**, *4*, 6587.

[27] L. H. Hess, M. Jansen, V. Maybeck, M. V. Hauf, M. Seifert, M. Stutzmann, I. D. Sharp, A. Offenhäusser, J. A. Garrido, *Adv. Mater.* **2011**, *23*, 5045.

[28] O. N. Ruiz, K. A. S. Fernando, B. Wang, N. A. Brown, P. G. Luo, N. D. McNamara, M. Vangsness, Y.-P. Sun, C. E. Bunker, *ACS Nano* **2011**, *5*, 8100.

[29] Y. Zhang, S. F. Ali, E. Dervishi, Y. Xu, Z. Li, D. Casciano, A. S. Biris, *ACS Nano* **2010**, *4*, 3181.

[30] A. Bendali, L. H. Hess, M. Seifert, V. Forster, A.-F. Stephan, J. A. Garrido, S. Picaud, *Adv. Healthcare Mater.* **2013**, *2*, 929.

[31] N. Li, X. Zhang, Q. Song, R. Su, Q. Zhang, T. Kong, L. Liu, G. Jin, M. Tang, G. Cheng, *Biomaterials* **2011**, *32*, 9374.

[32] S. Agarwal, X. Zhou, F. Ye, Q. He, G. C. K. Chen, J. Soo, F. Boey, H. Zhang, P. Chen, *Langmuir* **2010**, *26*, 2244.

[33] G. Y. Chen, D. W. P. Pang, S. M. Hwang, H. Y. Tuan, Y. C. Hu, *Biomaterials* **2012**, *33*, 418.

[34] C.-H. Chen, C.-T. Lin, W.-L. Hsu, Y.-C. Chang, S.-R. Yeh, L.-J. Li, D.-J. Yao, *Nanomedicine* **2013**, *9*, 600.
[35] D. Kuzum, H. Takano, E. Shim, J. C. Reed, H. Juul, A. G. Richardson, J. de Vries, H. Bink, M. A. Dichter, T. H. Lucas, D. A. Coulter, E. Cubukcu, B. Litt, *Nat. Commun.* **2014**, *5*.
[36] D.-W. Park, A. A. Schendel, S. Mikael, S. K. Brodnick, T. J. Richner, J. P. Ness, M. R. Hayat, F. Atry, S. T. Frye, R. Pashaie, S. Thongpang, Z. Ma, J. C. Williams, *Nat. Commun.* **2014**, *5*.
[37] D.-W. Park, S. K. Brodnick, J. P. Ness, F. Atry, L. Krugner-Higby, A. Sandberg, S. Mikael, T. J. Richner, J. Novello, H. Kim, D.-H. Baek, J. Bong, S. T. Frye, S. Thongpang, K. I. Swanson, W. Lake, R. Pashaie, J. C. Williams, Z. Ma, *Nat. Protoc.* **2016**, *11*, 2201.
[38] N. V. Apollo, M. I. Maturana, W. Tong, D. A. X. Nayagam, M. N. Shivdasani, J. Foroughi, G. G. Wallace, S. Prawer, M. R. Ibbotson, D. J. Garrett, *Adv. Funct. Mater.* **2015**, *25*, 3551.
[39] R. Kempaiah, A. Chung, V. Maheshwari, *ACS Nano* **2011**, *5*, 6025.
[40] M. Deng, X. Yang, M. Silke, W. Qiu, M. Xu, G. Borghs, H. Chen, *Sens. Actuators B* **2011**, *158*, 176.
[41] X. Luo, C. L. Weaver, S. Tan, X. T. Cui, *J. Mater. Chem. B* **2013**, *1*, 1340.
[42] H.-C. Tian, J.-Q. Liu, D.-X. Wei, X.-Y. Kang, C. Zhang, J.-C. Du, B. Yang, X. Chen, H.-Y. Zhu, Y.-N. NuLi, C.-S. Yang, *Biomaterials* **2014**, *35*, 2120.
[43] P. C. Sherrell, B. C. Thompson, J. K. Wassei, A. A. Gelmi, M. J. Higgins, R. B. Kaner, G. G. Wallace, *Adv. Funct. Mater.* **2014**, *24*, 769.
[44] X. Liu, A. L. Miller Ii, S. Park, B. E. Waletzki, A. Terzic, M. J. Yaszemski, L. Lu, *J. Mater. Chem. B* **2016**, *4*, 6930.
[45] H. W. Kroto, J. R. Heath, S. C. O'Brien, R. F. Curl, R. E. Smalley, *Nature* **1985**, *318*, 162.
[46] S. Iijima, *Nature* **1991**, *354*, 56.
[47] J. J. Pancrazio, *Nanomedicine* **2008**, *3*, 823.
[48] C. M. Voge, J. P. Stegemann, *J. Neural Eng.* **2011**, *8*, 011001.
[49] M. P. Mattson, R. C. Haddon, A. M. Rao, *J. Mol. Neurosci.* **2000**, *14*, 175.
[50] V. Lovat, D. Pantarotto, L. Lagostena, B. Cacciari, M. Grandolfo, M. Righi, G. Spalluto, M. Prato, L. Ballerini, *Nano Lett.* **2005**, *5*, 1107.
[51] H. Hu, Y. Ni, V. Montana, R. C. Haddon, V. Parpura, *Nano Lett.* **2004**, *4*, 507.
[52] J. Xie, L. Chen, K. R. Aatre, M. Srivatsan, V. K. Varadan, *Smart Mater. Struct.* **2006**, *15*, N85.
[53] P. Galvan-Garcia, E. W. Keefer, F. Yang, M. Zhang, S. Fang, A. A. Zakhidov, R. H. Baughman, M. I. Romero, *J. Biomater. Sci. Polym. Ed.* **2007**, *18*, 1245.
[54] L. P. Zanello, B. Zhao, H. Hu, R. C. Haddon, *Nano Lett.* **2006**, *6*, 562.
[55] K. Matsumoto, C. Sato, Y. Naka, R. Whitby, N. Shimizu, *Nanotechnology* **2010**, *21*, 115101.
[56] M. K. Gheith, V. A. Sinani, J. P. Wicksted, R. L. Matts, N. A. Kotov, *Adv. Mater.* **2005**, *17*, 2663.
[57] E. B. Malarkey, K. A. Fisher, E. Bekyarova, W. Liu, R. C. Haddon, V. Parpura, *Nano Lett.* **2009**, *9*, 264.
[58] T.-I. Chao, S. Xiang, C.-S. Chen, W.-C. Chin, A. J. Nelson, C. Wang, J. Lu, *Biochem. Biophys. Res. Commun.* **2009**, *384*, 426.
[59] N. W. S. Kam, E. Jan, N. A. Kotov, *Nano Lett.* **2009**, *9*, 273.
[60] H. Chen, L. Guo, A. R. Ferhan, D.-H. Kim, *J. Phys. Chem. C* **2011**, *115*, 5492.
[61] M. A. Correa-Duarte, N. Wagner, J. Rojas-Chapana, C. Morsczeck, M. Thie, M. Giersig, *Nano Lett.* **2004**, *4*, 2233.
[62] T. D. B. Nguyen-Vu, H. Chen, A. M. Cassell, R. Andrews, M. Meyyappan, J. Li, *Small* **2006**, *2*, 89.
[63] A. F. Quigley, J. M. Razal, M. Kita, R. Jalili, A. Gelmi, A. Penington, R. Ovalle-Robles, R. H. Baughman, G. M. Clark, G. G. Wallace, R. M. I. Kapsa, *Adv. Healthcare Mater.* **2012**, *1*, 801.
[64] T. Gabay, et al., *Nanotechnology* **2007**, *18*, 035201.
[65] E. Keefer, B. Botterman, M. Romero, A. Rossi, G. Gross, *Nat. Nanotechnol.* **2008**, *3*, 434.
[66] G. Gabriel, R. Gómez, M. Bongard, N. Benito, E. Fernández, R. Villa, *Biosens. Bioelectron.* **2009**, *24*, 1942.

[67] Y.-C. Chen, et al., *J. Neural Eng.* **2011**, *8*, 034001.
[68] J. H. Shin, G. B. Kim, E. J. Lee, T. An, K. Shin, S. E. Lee, W. Choi, S. Lee, C. Latchoumane, H.-S. Shin, G. Lim, *Adv. Healthcare Mater.* **2014**, *3*, 245.
[69] S.-J. Yen, W.-L. Hsu, Y.-C. Chen, H.-C. Su, Y.-C. Chang, H. Chen, S.-R. Yeh, T.-R. Yew, *Biosens. Bioelectron.* **2011**, *26*, 4124.
[70] H. S. Mandal, G. L. Knaack, H. Charkhkar, D. G. McHail, J. S. Kastee, T. C. Dumas, N. Peixoto, J. F. Rubinson, J. J. Pancrazio, *Acta Biomater.* **2014**, *10*, 2446.
[71] S. Chen, W. Pei, Q. Gui, R. Tang, Y. Chen, S. Zhao, H. Wang, H. Chen, *Sens. Actuators A* **2013**.
[72] E. Castagnola, A. Ansaldo, E. Maggiolini, G. N. Angotzi, M. Skrap, D. Ricci, L. Fadiga, *ACS Nano* **2013**, *7*, 3887.
[73] T. D. Y. Kozai, K. Catt, Z. Du, K. Na, O. Srivannavit, R. M. Haque, J. Seymour, K. D. Wise, E. Yoon, X. T. Cui, *IEEE Trans. Biomed. Eng.*, **2016**, *63*, 111.
[74] C. L. Kolarcik, K. Catt, E. Rost, I. N. Albrecht, D. Bourbeau, Z. Du, T. D. Y. Kozai, X. Luo, D. J. Weber, X. T. Cui, *J. Neural Eng.* **2015**, *12*, 016008.
[75] G. Piret, C. Hébert, J.-P. Mazellier, L. Rousseau, E. Scorsone, M. Cottance, G. Lissorgues, M. O. Heuschkel, S. Picaud, P. Bergonzo, B. Yvert, *Biomaterials* **2015**, *53*, 173.
[76] S. Musa, D. R. Rand, D. J. Cott, J. Loo, C. Bartic, W. Eberle, B. Nuttin, G. Borghs, *ACS Nano* **2012**, *6*, 4615.
[77] A. V. Liopo, M. P. Stewart, J. Hudson, J. M. Tour, T. C. Pappas, *J. Nanosci. Nanotechnol.* **2006**, *6*, 1365.
[78] K. Wang, H. A. Fishman, H. Dai, J. S. Harris, *Nano Lett.* **2006**, *6*, 2043.
[79] A. Mazzatenta, M. Giugliano, S. Campidelli, L. Gambazzi, L. Businaro, H. Markram, M. Prato, L. Ballerini, *J. Neurosci.* **2007**, *27*, 6931.
[80] M. K. Gheith, T. C. Pappas, A. V. Liopo, V. A. Sinani, B. S. Shim, M. Motamedi, J. P. Wicksted, N. A. Kotov, *Adv. Mater.* **2006**, *18*, 2975.
[81] R. Samba, T. Herrmann, G. Zeck, *J. Neural Eng.* **2015**, *12*, 016014.
[82] F. Vitale, S. R. Summerson, B. Aazhang, C. Kemere, M. Pasquali, *ACS Nano* **2015**, *9*, 4465.
[83] J. Heinze, B. A. Frontana-Uribe, S. Ludwigs, *Chem. Rev.* **2010**, *110*, 4724.
[84] G. G. Wallace, S. Moulton, R. M. I. Kapsa, M. Higgins, *Organic Bionics*, Wiley-VCH, Weinheim, **2012**.
[85] V. S. Polikov, P. A. Tresco, W. M. Reichert, *J. Neurosci. Methods* 2005, 148, 1.
[86] M. Berggren, A. Richter-Dahlfors, *Adv. Mater.* **2007**, *19*, 3201.
[87] R. A. Green, N. H. Lovell, G. G. Wallace, L. A. Poole-Warren, *Biomaterials* **2008**, *29*, 3393; S. F. Cogan, *Annu. Rev. Biomed. Eng.* **2008**, *10*, 275; R. A. Green, S. Baek, L. A. Poole-Warren, P. J. Martens, *Sci. Technol. Adv. Mater.* **2010**, *11*, 014107; R. M. Owens, G. G. Malliaras, *MRS Bull.* **2010**, *35*, 449; R. Ravichandran, S. Sundarrajan, J. R. Venugopal, S. Mukherjee, S. Ramakrishna, *J. R. Soc. Interface* **2010**, *7*, S559; J. H. Lee, H. Kim, J. H. Kim, S.-H. Lee, *Lab Chip* **2016**, *16*, 959.
[88] C. E. Schmidt, V. R. Shastri, J. P. Vacanti, R. Langer, *Proc. Natl. Acad. Sci. USA* **1997**, *94*, 8948.
[89] D. H. Kim, S. M. Richardson-Burns, J. L. Hendricks, C. Sequera, D. C. Martin, *Adv. Funct. Mater.* **2007**, *17*, 79.
[90] A. Kotwal, C. E. Schmidt, *Biomaterials* **2001**, *22*, 1055.
[91] R. A. Green, N. H. Lovell, L. A. Poole-Warren, *Biomaterials* **2009**, *30*, 3637.
[92] R. A. Green, N. H. Lovell, L. A. Poole-Warren, *Acta Biomater.* **2010**, *6*, 63.
[93] Y. Lu, T. Li, X. Zhao, M. Li, Y. Cao, H. Yang, Y. Y. Duan, *Biomaterials* **2010**, *31*, 5169.
[94] X. Liu, Z. Yue, M. J. Higgins, G. G. Wallace, Biomaterials 2011, 32, 7309; P. J. Molino, Z. Yue, B. Zhang, A. Tibbens, X. Liu, R. M. I. Kapsa, M. J. Higgins, G. G. Wallace, *Adv. Mater. Interfaces* **2014**, *1*, 1300122.
[95] X. Cui, D. C. Martin, *Sens. Actuators B* **2003**, *89*, 92.
[96] D. T. Simon, S. Kurup, K. C. Larsson, R. Hori, K. Tybrandt, M. Goiny, E. W. H. Jager, M. Berggren, B. Canlon, A. Richter-Dahlfors, *Nat. Mater.* **2009**, *8*, 742.

[97] X. Cui, V. A. Lee, Y. Raphael, J. A. Wiler, J. F. Hetke, D. J. Anderson, D. C. Martin, *J. Biomed. Mater. Res.* **2001**, *56*, 261.
[98] Y. Xiao, D. Martin, X. Cui, M. Shenai, *Appl. Biochem. Biotechnol.* **2006**, *128*, 117.
[99] M. Mattioli-Belmonte, F. Gabbanelli, M. Marcaccio, F. Giantomassi, R. Tarsi, D. Natali, A. Callegari, F. Paolucci, G. Biagini, *Mater. Sci. Eng. C* **2005**, *25*, 43.
[100] T. Nyberg, A. Shimada, K. Torimitsu, *J. Neurosci. Methods* **2007**, *160*, 16.
[101] R. Wadhwa, C. F. Lagenaur, X. T. Cui, *J. Controlled Release* **2006**, *110*, 531.
[102] W. R. Stauffer, et al., *J. Neural Eng.* **2011**, *8*, 044001.
[103] X. Luo, C. L. Weaver, D. D. Zhou, R. Greenberg, X. T. Cui, *Biomaterials* **2011**, *32*, 5551.
[104] J. E. Collazos-Castro, G. R. Hernández-Labrado, J. L. Polo, C. García-Rama, *Biomaterials* **2013**, *34*, 3603.
[105] R. T. Richardson, B. Thompson, S. Moulton, C. Newbold, M. G. Lum, A. Cameron, G. Wallace, R. Kapsa, G. Clark, S. O'Leary, *Biomaterials* **2007**, *28*, 513.
[106] B. C. Thompson, S. E. Moulton, R. T. Richardson, G. G. Wallace, *Biomaterials* **2011**, *32*, 3822.
[107] L. K. Povlich, J. C. Cho, M. K. Leach, J. M. Corey, J. Kim, D. C. Martin, *Biochim. Biophys. Acta* 2013, 1830, 4288.
[108] B. Zhu, S.-C. Luo, H. Zhao, H.-A. Lin, J. Sekine, A. Nakao, C. Chen, Y. Yamashita, H.-h. Yu, *Nat. Commun.* **2014**, 5.

[131] R. A. Green, P. B. Matteucci, R. T. Hassarati, B. Giraud, C. W. D. Dodds, S. Chen, P. J. Byrnes-Preston, G. J. Suaning, L. A. Poole-Warren, N. H. Lovell, *J. Neural Eng.* **2013**, *10*, 016009.
[132] A. R. Harris, S. J. Morgan, J. Chen, R. M. I. Kapsa, G. G. Wallace, A. G. Paolini, *J. Neural Eng.* **2013**, *10*, 016004.
[133] A. R. Harris, S. J. Morgan, G. G. Wallace, A. G. Paolini, *J. Vis. Exp.* **2014**, e51084.
[134] A. R. Harris, P. J. Molino, R. M. I. Kapsa, G. M. Clark, A. G. Paolini, G. G. Wallace, *Anal. Chem:* **2015**, *87*, 738; A. R. Harris, P. J. Molino, R. M. I. Kapsa, G. M. Clark, A. G. Paolini, G. G. Wallace, *Synth. Met.* **2016**, *220*, 394; A. R. Harris, P. J. Molino, A. G. Paolini, G. G. Wallace, *Electrochim. Acta* **2016**, *197*, 99.
[135] B. H. Brown, *Med. Biol. Eng.* **1968**, *6*, 493.
[136] A. R. Harris, P. J. Molino, R. M. I. Kapsa, G. M. Clark, A. G. Paolini, G. G. Wallace, Analyst 2015, 140, 3164; A. R. Harris, R. Hutchinson, P. J. Molino, R. M. I. Kapsa, G. M. Clark, A. G. Paolini, G. G. Wallace, *J. Electrochem. Soc.* **2016**, *163*, H534; A. R. Harris, P. J. Molino, A. G. Paolini, G. G. Wallace, *Synth. Met.* **2016**, *222*, 338.
[137] D. Khodagholy, T. Doublet, M. Gurfinkel, P. Quilichini, E. Ismailova, P. Leleux, T. Herve, S. Sanaur, C. Bernard, G. G. Malliaras, *Adv. Mater.* **2011**, *23*, H268.
[138] A. A. Guex, N. Vachicouras, A. E. Hight, M. C. Brown, D. J. Lee, S. P. Lacour, *J. Mater. Chem. B* **2015**, *3*, 5021.
[139] J. F. Maya-Vetencourt, D. Ghezzi, M. R. Antognazza, E. Colombo, M. Mete, P. Feyen, A. Desii, A. Buschiazzo, M. Di Paolo, S. Di Marco, F. Ticconi, L. Emionite, D. Shmal, C. Marini, I. Donelli, G. Freddi, R. Maccarone, S. Bisti, G. Sambuceti, G. Pertile, G. Lanzani, F. Benfenati, *Nat. Mater.* **2017**, advance online publication.
[140] S. M. Richardson-Burns, J. L. Hendricks, B. Foster, L. K. Povlich, D.-H. Kim, D. C. Martin, *Biomaterials* **2007**, *28*, 1539.
[141] S. M. Richardson-Burns, J. L. Hendricks, D. C. Martin, *J. Neural Eng.* **2007**, L6.
[142] L. Ouyang, C. L. Shaw, C.-c. Kuo, A. L. Griffin, D. C. Martin, *J. Neural Eng.* **2014**, *11*, 026005.
[143] D. Khodagholy, T. Doublet, P. Quilichini, M. Gurfinkel, P. Leleux, A. Ghestem, E. Ismailova, T. Hervé, S. Sanaur, C. Bernard, G. G. Malliaras, *Nat. Commun.* **2013**, *4*, 1575.
[144] P. Leleux, J. Rivnay, T. Lonjaret, J.-M. Badier, C. Bénar, T. Hervé, P. Chauvel, G. G. Malliaras, *Adv. Healthcare Mater.* **2015**, *4*, 142.
[145] A. Williamson, M. Ferro, P. Leleux, E. Ismailova, A. Kaszas, T. Doublet, P. Quilichini, J. Rivnay, B. Rózsa, G. Katona, C. Bernard, G. G. Malliaras, *Adv. Mater.* **2015**, *27*, 4405.

[146] G. Baranauskas, E. Maggiolini, E. Castagnola, A. Ansaldo, A. Mazzoni, G. N. Angotzi, A. Vato, D. Ricci, S. Panzeri, L. Fadiga, *J. Neural Eng.* **2011**, *8*, 066013.
[147] D. M. Fernandes, C. M. A. Brett, A. M. V. Cavaleiro, *J. Electroanal. Chem.* **2011**, *660*, 50.
[148] Z. J. Du, X. Luo, C. L. Weaver, X. T. Cui, *J. Mater. Chem. C* **2015**, *3*, 6515.
[149] V. Armel, O. Winther-Jensen, R. Kerr, D. R. MacFarlane, B. Winther-Jensen, *J. Mater. Chem.* **2012**, *22*, 19767.
[150] L. Pan, G. Yu, D. Zhai, H. R. Lee, W. Zhao, N. Liu, H. Wang, B. C.-K. Tee, Y. Shi, Y. Cui, Z. Bao, *Proc. Natl. Acad. Sci. USA* **2012**, *109*, 9287; Y. Zhao, B. Liu, L. Pan, G. Yu, *Energy Environ. Sci.* **2013**, *6*, 2856.
[151] T. M. Higgins, S. E. Moulton, K. J. Gilmore, G. G. Wallace, M. in het Panhuis, *Soft Matter* **2011**, *7*, 4690.
[152] M. Sasaki, B. C. Karikkineth, K. Nagamine, H. Kaji, K. Torimitsu, M. Nishizawa, *Adv. Healthcare Mater.* **2014**, *3*, 1919.
[153] G. L. M. Cheong, K. S. Lim, A. Jakubowicz, P. J. Martens, L. A. Poole-Warren, R. A. Green, *Acta Biomater.* **2014**, *10*, 1216.
[154] D. Mawad, A. Artzy-Schnirman, J. Tonkin, J. Ramos, S. Inal, M. M. Mahat, N. Darwish, L. Zwi-Dantsis, G. G. Malliaras, J. J. Gooding, A. Lauto, M. M. Stevens, *Chem. Mat.* **2016**, *28*, 6080.
[155] M. R. Abidian, E. D. Daneshvar, B. M. Egeland, D. R. Kipke, P. S. Cederna, M. G. Urbanchek, *Adv. Healthcare Mater.* **2012**, *1*, 762.
[156] M. Zhu, C. Zeng, J. Ye, *Electroanalysis* **2011**, *23*, 907.
[157] K. Jackowska, P. Krysinski, *Anal. Bioanal. Chem.* **2013**, *405*, 3753.
[158] C. B. Jacobs, M. J. Peairs, B. J. Venton, *Anal. Chim. Acta* **2010**, 662, 105.
[159] J. Wang, R. P. Deo, P. Poulin, M. Mangey, *J. Am. Chem. Soc.* **2003**, *125*, 14706; L. Viry, A. Derre, P. Poulin, A. Kuhn, *Phys. Chem. Chem. Phys.* **2010**, *12*, 9993; N. Xiao, B. J. Venton, *Anal. Chem.* **2012**, *84*, 7816; C. B. Jacobs, T. L. Vickrey, B. J. Venton, *Analyst* **2011**, *136*, 3557; A. C. Schmidt, X. Wang, Y. Zhu, L. A. Sombers, *ACS Nano* **2013**, *7*, 7864.
[160] L. Viry, A. Derré, P. Garrigue, N. Sojic, P. Poulin, A. Kuhn, *Anal. Bioanal. Chem.* **2007**, *389*, 499.
[161] I. Suzuki, M. Fukuda, K. Shirakawa, H. Jiko, M. Gotoh, *Biosens. Bioelectron.* **2013**, *49*, 270.
[162] W. Harreither, R. Trouillon, P. Poulin, W. Neri, A. G. Ewing, G. Safina, *Anal. Chem.* **2013**, *85*, 7447.
[163] S. Y. Yang, B. N. Kim, A. A. Zakhidov, P. G. Taylor, J.-K. Lee, C. K. Ober, M. Lindau, G. G. Malliaras, *Adv. Mater.* **2011**, *23*, H184.
[164] T. T. C. Tseng, H. G. Monbouquette, *J. Electroanal. Chem.* **2012**, *682*, 141.
[165] G. Fabregat, J. Casanovas, E. Redondo, E. Armelin, C. Aleman, *Phys. Chem. Chem. Phys.* **2014**, *16*, 7850.
[166] X. Sun, Z. Liu, K. Welsher, J. T. Robinson, A. Goodwin, S. Zaric, H. Dai, *Nano Res.* **2008**, *1*, 203.
[167] L. Zhang, J. Xia, Q. Zhao, L. Liu, Z. Zhang, *Small* **2010**, *6*, 537.
[168] N. Alba, Z. Du, K. Catt, T. Kozai, X. Cui, *Biosensors* **2015**, *5*, 618; B. Zhang, P. J. Molino, A. R. Harris, Z. Yue, S. E. Moulton, G. G. Wallace, *J. Mater. Chem. B* **2016**, *4*, 2570; M. R. Abidian, D. C. Martin, *Adv. Funct. Mater.* **2009**, *19*, 573.
[169] J. A. Goding, A. D. Gilmour, P. J. Martens, L. A. Poole-Warren, R. A. Green, *J. Mater. Chem. B* **2015**, *3*, 5058.
[170] R. T. Richardson, A. K. Wise, B. C. Thompson, B. O. Flynn, P. J. Atkinson, N. J. Fretwell, J. B. Fallon, G. G. Wallace, R. K. Shepherd, G. M. Clark, S. J. O'Leary, *Biomaterials* **2009**, *30*, 2614.
[171] J. D. Green, *Nature* **1958**, *182*, 962.
[172] H. J. Reitböck, G. Werner, *Cell. Mol. Life Sci.* **1983**, *39*, 339.
[173] O. P. Hamill, A. Marty, E. Neher, B. Sakmann, F. J. Sigworth, *Pflugers Arch. – Eur. J. Physiol.* **1981**, *391*, 85.
[174] K. Najafi, J. Ji, K. D. Wise, IEEE Trans. Biomed. Eng. **1990**, *37*, 1; P. K. Campbell, K. E. Jones, R. J. Huber, K. W. Horch, R. A. Normann, *IEEE Trans. Biomed. Eng.* **1991**, *38*, 758.

[175] J. F. Hetke, J. C. Williams, D. S. Pellinen, R. J. Vetter, D. R. Kipke, "3-D silicon probe array with hybrid polymer interconnect for chronic cortical recording", presented at *Neural Engineering, 2003. Conference Proceedings. First International IEEE EMBS Conference on*, 20-22 March 2003, 2003.
[176] A. Branner, R. B. Stein, E. Fernandez, Y. Aoyagi, R. A. Normann, *IEEE Trans. Biomed. Eng*. **2004**, *51*, 146.
[177] D.-H. Kim, J. Viventi, J. J. Amsden, J. Xiao, L. Vigeland, Y.-S. Kim, J. A. Blanco, B. Panilaitis, E. S. Frechette, D. Contreras, D. L. Kaplan, F. G. Omenetto, Y. Huang, K.-C. Hwang, M. R. Zakin, B. Litt, J. A. Rogers, *Nat. Mater.* **2010**, *9*, 511.
[178] B. Rubehn, C. Bosman, R. Oostenveld, P. Fries, T. Stieglitz, *J. Neural Eng.* **2009**, *6*, 036003.
[179] J. P. Abid, A. W. Wark, P. F. Brevet, H. H. Girault, *Chem. Commun.* **2002**, 792.
[180] S. Lee, Y. Inoue, D. Kim, A. Reuveny, K. Kuribara, T. Yokota, J. Reeder, M. Sekino, T. Sekitani, Y. Abe, T. Someya, *Nat. Commun.* **2014**, *5*.
[181] J. Liu, T.-M. Fu, Z. Cheng, G. Hong, T. Zhou, L. Jin, M. Duvvuri, Z. Jiang, P. Kruskal, C. Xie, Z. Suo, Y. Fang, C. M. Lieber, *Nat. Nanotechnol.* **2015**, *10*, 629.
[182] C. Xie, J. Liu, T.-M. Fu, X. Dai, W. Zhou, C. M. Lieber, *Nat. Mater.* **2015**, *14*, 1286; T.-M. Fu, G. Hong, T. Zhou, T. G. Schuhmann, R. D. Viveros, C. M. Lieber, *Nat. Methods* **2016**, *13*, 875.
[183] T. J. Oxley, N. L. Opie, S. E. John, G. S. Rind, S. M. Ronayne, T. L. Wheeler, J. W. Judy, A. J. McDonald, A. Dornom, T. J. H. Lovell, C. Steward, D. J. Garrett, B. A. Moffat, E. H. Lui, N. Yassi, B. C. V. Campbell, Y. T. Wong, K. E. Fox, E. S. Nurse, I. E. Bennett, S. H. Bauquier, K. A. Liyanage, N. R. van der Nagel, P. Perucca, A. Ahnood, K. P. Gill, B. Yan, L. Churilov, C. R. French, P. M. Desmond, M. K. Horne, L. Kiers, S. Prawer, S. M. Davis, A. N. Burkitt, P. J. Mitchell, D. B. Grayden, C. N. May, T. J. O'Brien, *Nat. Biotechol.* **2016**, *34*, 320.
[184] N. L. Opie, S. E. John, G. S. Rind, S. M. Ronayne, D. B. Grayden, A. N. Burkitt, C. N. May, T. J. O'Brien, T. J. Oxley, *J. Neural Eng.* **2016**, *13*, 046020.
[185] H.-P. Cong, X.-C. Ren, P. Wang, S.-H. Yu, *Sci. Rep.* **2012**, *2*, 613.
[186] R. Jalili, S. H. Aboutalebi, D. Esrafilzadeh, R. L. Shepherd, J. Chen, S. Aminorroaya-Yamini, K. Konstantinov, A. I. Minett, J. M. Razal, G. G. Wallace, *Adv. Funct. Mater.* **2013**, *23*, 5345.
[187] B. Vigolo, A. Pénicaud, C. Coulon, C. Sauder, R. Pailler, C. Journet, P. Bernier, P. Poulin, *Science* **2000**, *290*, 1331.
[188] E. M. Scherr, A. G. MacDiarmid, S. K. Manohar, J. G. Masters, Y. Sun, X. Tang, M. A. Druy, P. J. Glatkowski, V. B. Cajipe, J. E. Fischer, K. R. Cromack, M. E. Jozefowicz, J. M. Ginder, R. P. McCall, A. J. Epstein, *Synth. Met.* **1991**, *41*, 735; C. H. Hsu, J. D. Cohen, R. F. Tietz, *Synth. Met.* **1993**, *59*, 37; H.-L. Wang, R. J. Romero, B. R. Mattes, Y. Zhu, M. J. Winokur, *J. Polym. Sci. Part B* **2000**, *38*, 194; S. J. Pomfret, P. N. Adams, N. P. Comfort, A. P. Monkman, *Polymer* **2000**, *41*, 2265.
[189] T. Takahashi, M. Ishihara, H. Okuzaki, *Synth. Met.* **2005**, *152*, 73.
[190] J. Foroughi, G. M. Spinks, G. G. Wallace, P. G. Whitten, *Synt. Met.* **2008**, *158*, 104.
[191] J. M. Razal, K. J. Gilmore, G. G. Wallace, *Adv. Funct. Mater.* **2008**, *18*, 61.[192] C. Lynam, S. E. Moulton, G. G. Wallace, *Adv. Mater.* **2007**, *19*, 1244.
[193] J. Foroughi, G. M. Spinks, G. G. Wallace, *J. Mater. Chem*. **2011**, *21*, 6421.
[194] A. F. Quigley, J. M. Razal, B. C. Thompson, S. E. Moulton, M. Kita, E. L. Kennedy, G. M. Clark, G. G. Wallace, R. M. I. Kapsa, *Adv. Mater.* **2009**, *21*, 4393.
[195] J. M. Razal, M. Kita, A. F. Quigley, E. Kennedy, S. E. Moulton, R. M. I. Kapsa, G. M. Clark, G. G. Wallace, *Adv. Funct. Mater.* **2009**, *19*, 3381.
[196] D. Esrafilzadeh, J. M. Razal, S. E. Moulton, E. M. Stewart, G. G. Wallace, *J. Controlled Release* **2013**, *169*, 313.
[197] A. Theron, E. Zussman, A. L. Yarin, *Nanotechnology* **2001**, *12*, 384.
[198] A. G. MacDiarmid, W. E. Jones, I. D. Norris, J. Gao, A. T. Johnson, N. J. Pinto, J. Hone, B. Han, F. K. Ko, H. Okuzaki, M. Llaguno, *Synth. Met.* **2001**, *119*, 27.
[199] Z.-M. Huang, Y. Z. Zhang, M. Kotaki, S. Ramakrishna, *Compos. Sci. Technol.* **2003**, *63*, 2223.
[200] F. Yang, R. Murugan, S. Wang, S. Ramakrishna, *Biomaterials* **2005**, *26*, 2603.

[201] J. Xie, M. R. MacEwan, S. M. Willerth, X. Li, D. W. Moran, S. E. Sakiyama-Elbert, Y. Xia, *Adv. Funct. Mater.* **2009**, *19*, 2312.
[202] M. H. Bolin, K. Svennersten, X. Wang, I. S. Chronakis, A. Richter-Dahlfors, E. W. H. Jager, M. Berggren, *Sens. Actuators B* **2009**, *142*, 451.
[203] S. I. Jeong, I. D. Jun, M. J. Choi, Y. C. Nho, Y. M. Lee, H. Shin, *Macromol. Biosci.* **2008**, *8*, 627.
[204] L. Y. Yeo, J. R. Friend, *J. Exper. Nanosci.* **2006**, *1*, 177.
[205] Y. Liu, K. J. Gilmore, J. Chen, V. Misoska, G. G. Wallace, *Chem. Mater.* **2007**, *19*, 2721.
[206] Z.-Q. Feng, T. Wang, B. Zhao, J. Li, L. Jin, *Adv. Mater.* **2015**, *27*, 6462.
[207] M. Zhang, S. Fang, A. A. Zakhidov, S. B. Lee, A. E. Aliev, C. D. Williams, K. R. Atkinson, R. H. Baughman, *Science* **2005**, *309*, 1215.
[208] M. Zhang, K. R. Atkinson, R. H. Baughman, *Science* **2004**, *306*, 1358.
[209] O. Ngamna, A. Morrin, A. J. Killard, S. E. Moulton, M. R. Smyth, G. G. Wallace, Langmuir 2007, 23, 8569; J. Jang, J. Ha, J. Cho, *Adv. Mater.* **2007**, *19*, 1772.
[210] M. F. Mabrook, C. Pearson, M. C. Petty, *Sens. Actuators B* **2006**, *115*, 547.
[211] M. F. Mabrook, C. Pearson, M. C. Petty, *Appl. Phys. Lett.* **2005**, *86*, 013507.
[212] J. Cho, K.-H. Shin, J. Jang, *Thin Solid Films* **2010**, *518*, 5066.
[213] T. Mustonen, K. Kordás, S. Saukko, G. Tóth, J. S. Penttilä, P. Helistö, H. Seppä, H. Jantunen, *Phys. Status Solidi (b)* **2007**, *244*, 4336; D. Aurore, B. Julien, B. Anne, K. Bertine, R.-D. Francine, N. Charles, *Nanotechnology* **2009**, *20*, 385701.
[214] E. B. Secor, P. L. Prabhumirashi, K. Puntambekar, M. L. Geier, M. C. Hersam, The Journal of *Phys. Chem. Lett.* **2013**, *4*, 1347; L. Huang, Y. Huang, J. Liang, X. Wan, Y. Chen, *Nano Res.* **2011**, *4*, 675.
[215] P. G. Campbell, L. E. Weiss, *Expert Opin. Biol. Ther.* **2007**, *7*, 1123.
[216] C. A. Mire, A. Agrawal, G. G. Wallace, P. Calvert, M. in het Panhuis, *J. Mater. Chem.* **2011**, *21*, 2671.
[217] G. C. Pidcock, M. in het Panhuis, *Adv. Funct. Mater.* **2012**, *22*, 4790.
[218] A. E. Jakus, E. B. Secor, A. L. Rutz, S. W. Jordan, M. C. Hersam, R. N. Shah, *ACS Nano* **2015**, *9*, 4636.
[219] S. Naficy, R. Jalili, S. H. Aboutalebi, R. A. Gorkin Iii, K. Konstantinov, P. C. Innis, G. M. Spinks, P. Poulin, G. G. Wallace, *Mater. Horizons* **2014**, *1*, 326.
[220] J. H. Kim, W. S. Chang, D. Kim, J. R. Yang, J. T. Han, G.-W. Lee, J. T. Kim, S. K. Seol, *Adv. Mater.* **2015**, *27*, 157.
[221] S. Sayyar, E. Murray, B. C. Thompson, J. Chung, D. L. Officer, S. Gambhir, G. M. Spinks, G. G. Wallace, *J. Mater. Chem. B* **2015**, *3*, 481.
[222] W. Hu, C. Peng, M. Lv, X. Li, Y. Zhang, N. Chen, C. Fan, Q. Huang, *ACS Nano* **2011**, *5*, 3693.
[223] A. Magrez, S. Kasas, V. Salicio, N. Pasquier, J. W. Seo, M. Celio, S. Catsicas, B. Schwaller, L. Forró, *Nano Lett.* **2006**, *6*, 1121.
[224] K. Donaldson, R. Aitken, L. Tran, V. Stone, R. Duffin, G. Forrest, A. Alexander, *Toxicol. Sci.* **2006**, *92*, 5.
[225] P. Cherukuri, C. J. Gannon, T. K. Leeuw, H. K. Schmidt, R. E. Smalley, S. A. Curley, R. B. Weisman, *Proc. Natl. Acad. Sci. USA* **2006**, *103*, 18882.
[226] A. Nimmagadda, K. Thurston, M. U. Nollert, P. S. McFetridge, *J. Biomed. Mater. Res. Part A* **2006**, 76A, 614.
[227] E. Oberdörster, *Environ. Health Perspect.* **2004**, *112*, 1058.
[228] S. Minnikanti, M. G. A. G. Pereira, S. Jaraiedi, K. Jackson, C. M. Costa-Neto, Q. Li, N. Peixoto, *J. Neural Eng.* **2010**, *7*, 016002.
[229] R. Balint, N. J. Cassidy, S. H. Cartmell, *Acta Biomater*. **2014**, *10*, 2341.
[230] S. Liu, J. Wang, D. Zhang, P. Zhang, J. Ou, B. Liu, S. Yang, *Appl. Surface Sci.* **2010**, *256*, 3427.
[231] M. Mattioli-Belmonte, G. Giavaresi, G. Biagini, L. Virgili, M. Giacomini, M. Fini, F. Giantomassi, D. Natali, P. Torricelli, R. Giardino, Int. J. Artif. Organs **2003**, *26*, 1077.
[232] C. H. Wang, Y. Q. Dong, K. Sengothi, K. L. Tan, E. T. Kang, *Synth. Met.* **1999**, *102*, 1313.

[233] P. Humpolicek, V. Kasparkova, P. Saha, J. Stejskal, *Synth. Met.* **2012**, *162*, 722.
[234] X. Wang, X. Gu, C. Yuan, S. Chen, P. Zhang, T. Zhang, J. Yao, F. Chen, G. Chen, *J. Biomed. Mater. Res. Part A* **2004**, 68A, 411.
[235] A. Vaitkuviene, V. Kaseta, J. Voronovic, G. Ramanauskaite, G. Biziuleviciene, A. Ramanaviciene, A. Ramanavicius, *J. Hazard. Mater.* **2013**, *250–251*, 167; S. Kim, W.-K. Oh, Y. S. Jeong, J.-Y. Hong, B.-R. Cho, J.-S. Hahn, J. Jang, *Biomaterials* **2011**, *32*, 2342.
[236] Y. S. Jeong, W.-K. Oh, S. Kim, J. Jang, *Biomaterials* **2011**, *32*, 7217.
[237] N. Ferraz, M. Strømme, B. Fellström, S. Pradhan, L. Nyholm, A. Mihranyan, *J. Biomed. Mater. Res. Part A* **2012**, *100A*, 2128.
[238] L. J. del Valle, F. Estrany, E. Armelin, R. Oliver, C. Alemán, *Macromol. Biosci.* **2008**, *8*, 1144.
[239] R. M. Miriani, M. R. Abidian, D. R. Kipke, "Cytotoxic analysis of the conducting polymer PEDOT using myocytes", presented at *2008 30th Annual International Conference of the IEEE Engineering in Medicine and Biology Society*, 20-25 Aug. 2008, 2008.
[240] M. Asplund, E. Thaning, J. Lundberg, A. C. Sandberg-Nordqvist, B. Kostyszyn, O. Inganäs, H. v. Holst, *Biomed. Mater.* **2009**, *4*, 045009.
[241] F. Pires, Q. Ferreira, C. A. V. Rodrigues, J. Morgado, F. C. Ferreira, *Biochim. Biophys. Acta* **2015**, *1850*, 1158.
[242] M. Mehrali, A. Thakur, C. P. Pennisi, S. Talebian, A. Arpanaei, M. Nikkhah, A. Dolatshahi-Pirouz, *Adv. Mater.* **2017**, *29*, 1603612.
[243] C. D. O'Connell, C. D. Bella, F. Thompson, C. Augustine, S. Beirne, R. Cornock, C. J. Richards, J. Chung, S. Gambhir, Z. Yue, J. Bourke, B. Zhang, A. Taylor, A. Quigley, R. Kapsa, P. Choong, G. G. Wallace, *Biofabrication* **2016**, *8*, 015019.

Figures

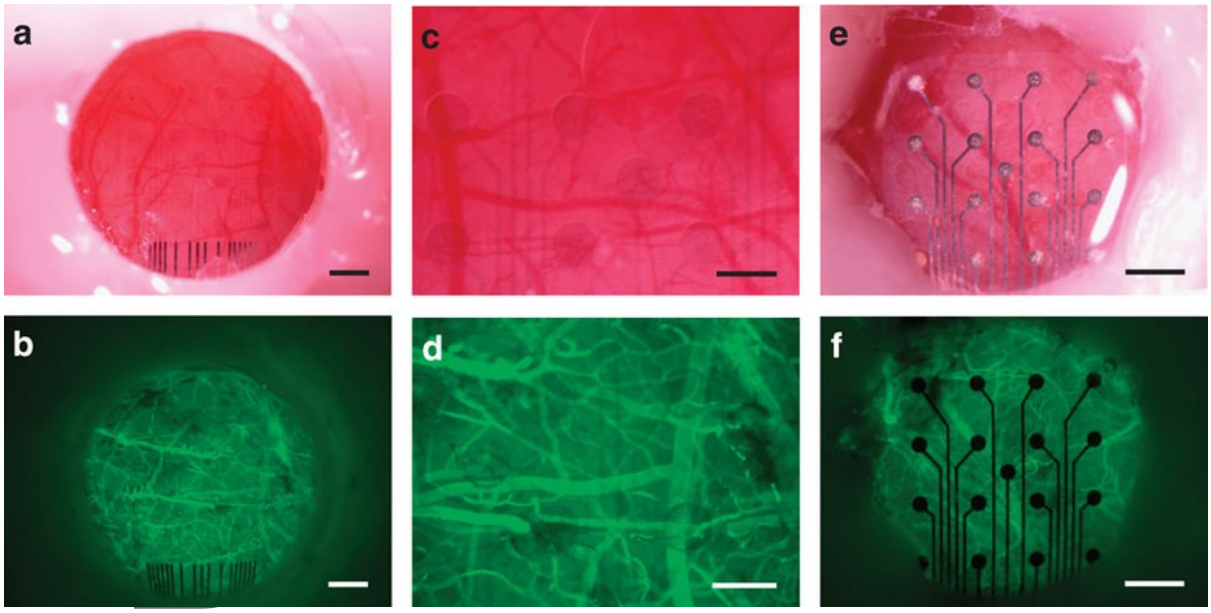

Figure 1. (a) Bright-field image of CLEAR device implanted on the cerebral cortex of a mouse beneath a cranial window. (b) Fluorescence image of same device shown in **a**. Mouse was given an intravenous injection of fluorescein isothiocyanate–dextran to fluorescently label the vasculature. (c,d) Higher magnification bright-field and fluorescence images of same device shown in **a** and **b**, respectively. (e,f) Bright-field and fluorescence images of standard rat-sized micro-ECoG arrays with platinum electrode sites, respectively. Scale bars, 500 µm (a,b), 250 µm (c,d), 750 µm (e,f). In vivo vasculature imaging was repeated in three rats, each with a CLEAR and platinum microECoG array. Reproduced with permission.[36] Copyright 2014, Nature Publishing Group.

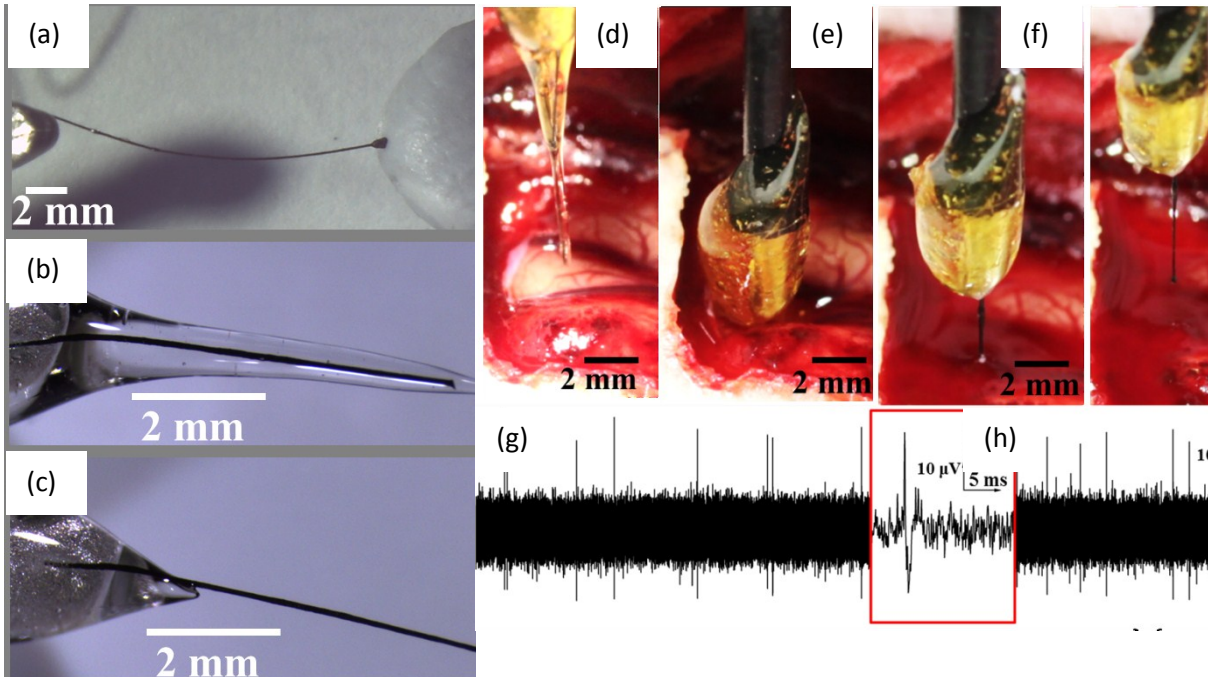

Figure 2. LCGO electrode (a) pressed into clay and released to demonstrate flexibility and elastic deformation (b) LCGO fiber (not laser ablated) encased in sucrose microneedle and (c) dissolved microneedle after 3 min in room temperature tap water. Flexible electrode insertion into feline visual cortex. (d) LCGO electrode is coated in a rigid sucrose carrier needle and (e) implanted into the brain. (f) LCGO electrode was removed from brain after 15 min of recording; sugar needle is completely dissolved. (g) Neural activity recorded within 20 s of implantation, confirming sucrose dissolution. (h) Magnified image of action potential recorded with LCGO electrode. Reproduced with permission.[38] Copyright 2015, Wiley-VCH.

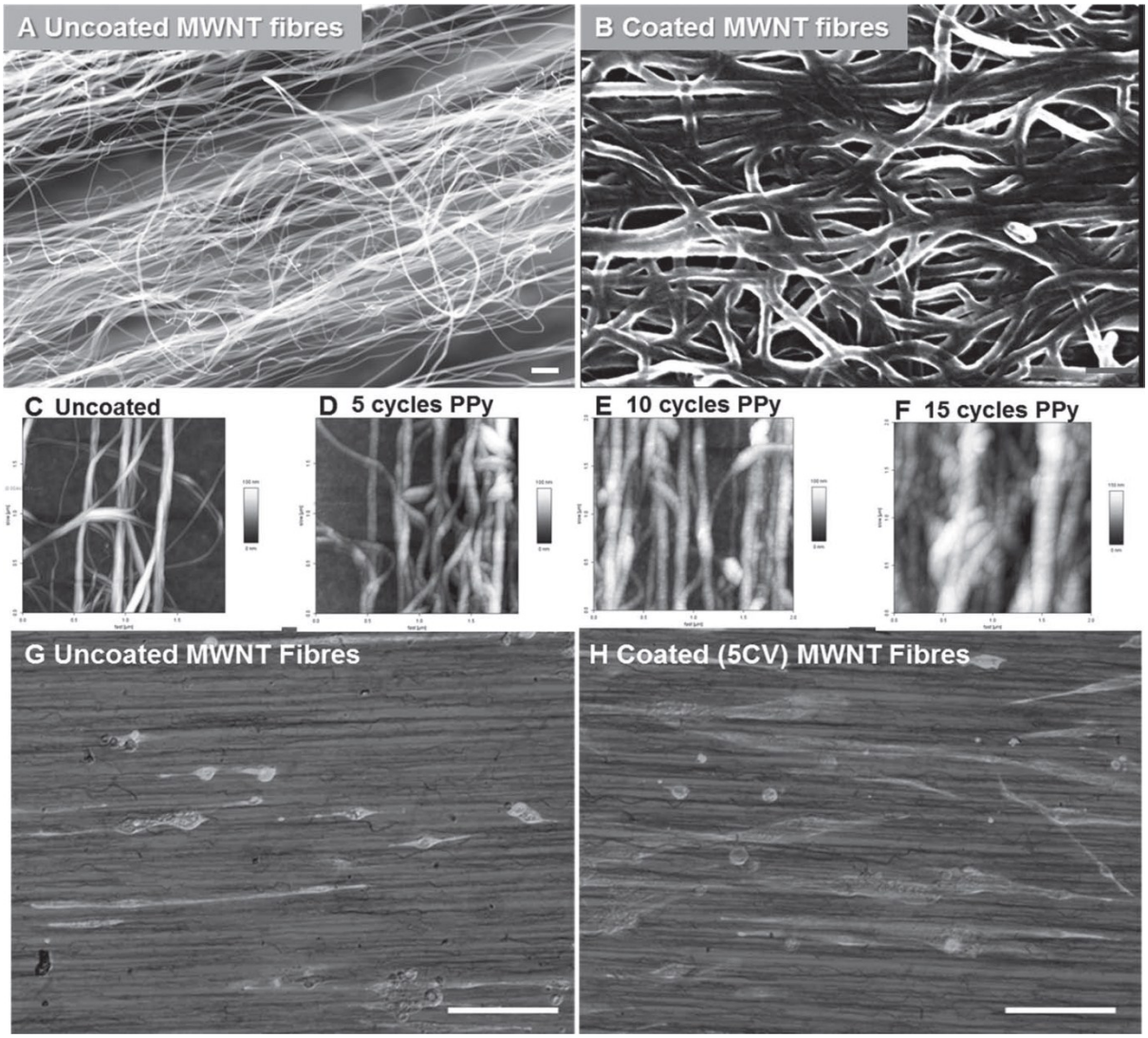

Figure 3. AFM and SEM images of MWNT and MWNT/PPy-*p*TS nanostructured scaffolds. MWNT were arrayed in a linear manner on Au mylar surfaces (a) to facilitate myotube orientation. PPy-*p*TS coating of MWNT fibers shows an even distribution of PPy-*p*TS (b). Increasing cycles of PPy-*p*TS deposition results in increased fiber thickness as demonstrated by AFM (c–f). The linear directionality of the uncoated (g) and coated MWNT fibers (h) can be seen by differential interference contrast light microscopy (myotubes are fluorescently labelled for desmin in panels g and h, scale bars represent 100 μm). Reproduced with permission.[63] Copyright 2012, Wiley-VCH.

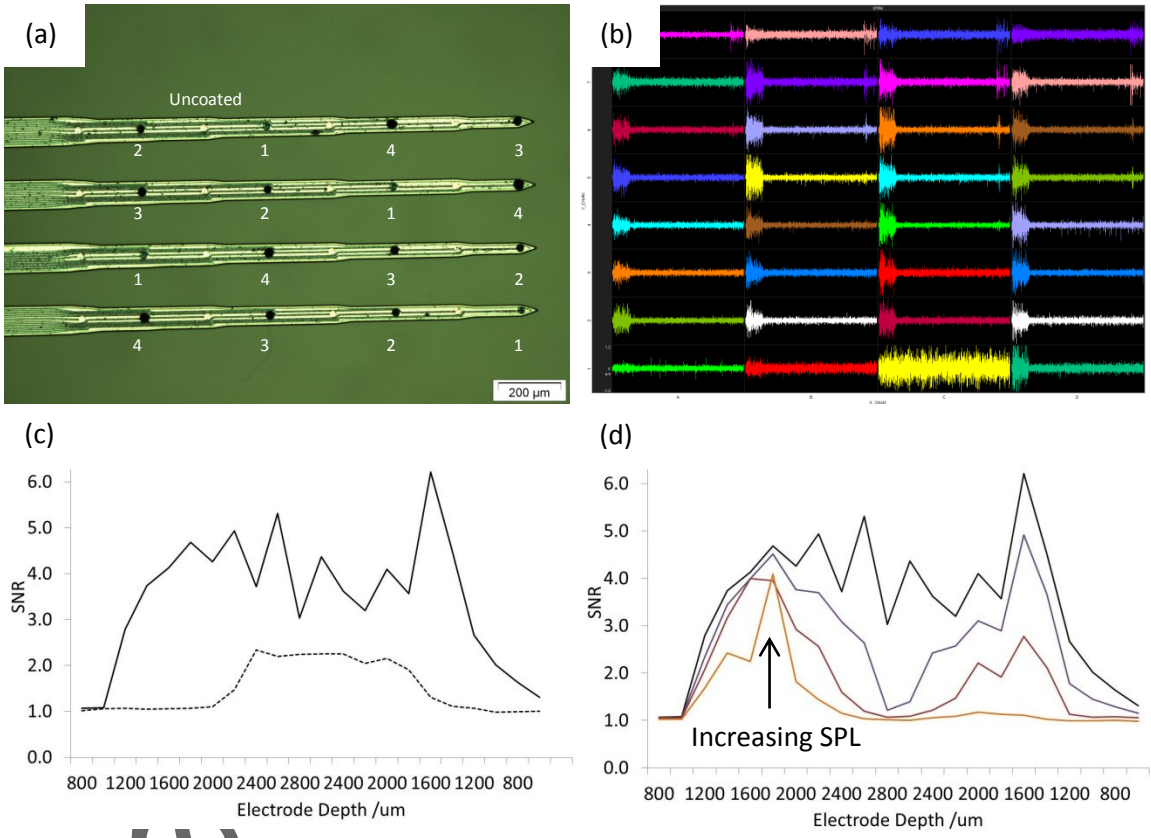

Figure 4. (a) Optical micrograph of a conducting polymer modified electrode array. The labels (1-4) represent four different coatings, enabling a statistical analysis of each coating within a single experiment. One uncoated electrode is also labelled. In this example, 1-4 are 15, 30, 45 and 60 s deposition times of PEDOT-pTS. (b) Streaming data measured at each electrode with 70 dB white noise bursts measured in the IC. Asterisks indicate the coated electrodes. (c) Signal to noise ratio during insertion and retraction of the electrode array into the IC. 70 dB white noise at representative uncoated (dashed) and conducting polymer coated (solid) electrodes and (d) different sound pressure levels (40-70 dB) on a conducting polymer coated electrode. Reproduced with permission[133]. Copyright 2014, MyJove Corp.

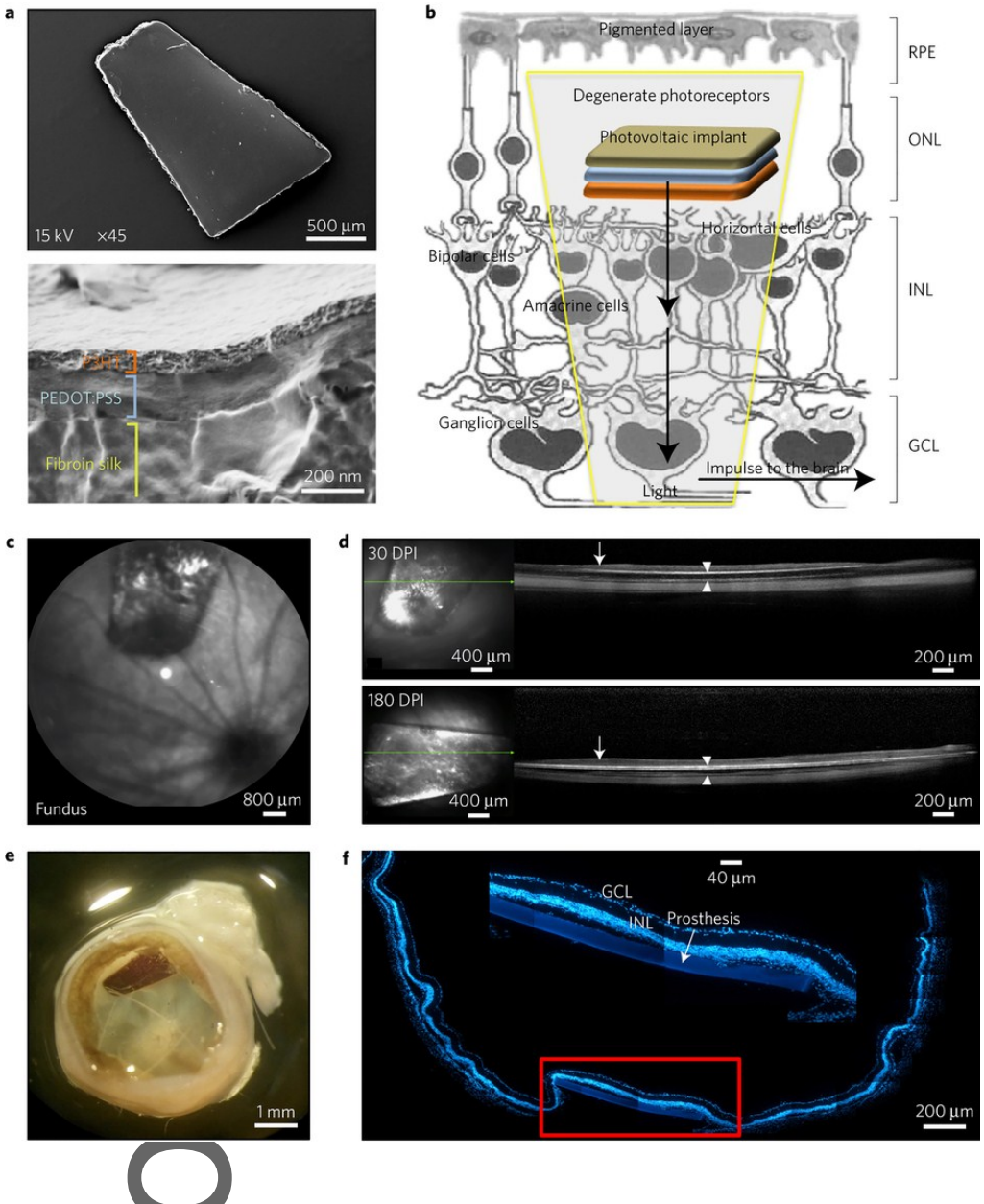

Figure 5. (a) Scanning electron microscopy images of the full prosthetic device (top) and of its cross-section at higher magnification showing the three-layered structure (bottom). (b) Scheme of the subretinal implant strategy. RPE, retinal pigment epithelium; ONL, outer nuclear layer; INL, inner nuclear layer; GCL, ganglion cell layer. (c) Sample confocal scanning laser ophthalmoscopy image of the surgical prosthesis placement in the eye fundus of a dystrophic RCS rat. (d) OCT analysis showing the strict contact between the retina (arrows) and the implant (arrowheads) at 30 and 180 dots per inch (DPI). No retinal detachments or breakages were observed. (e-f) Explanted eye fixed (e), stained with bisbenzimide and acquired by confocal microscopy (f) to identify retinal nuclear layers and the position of the device. The high-magnification image (red box) shows the integrity and location of the implant in the retina. Reproduced with permission.[139] Copyright 2017, Nature Publishing Group.

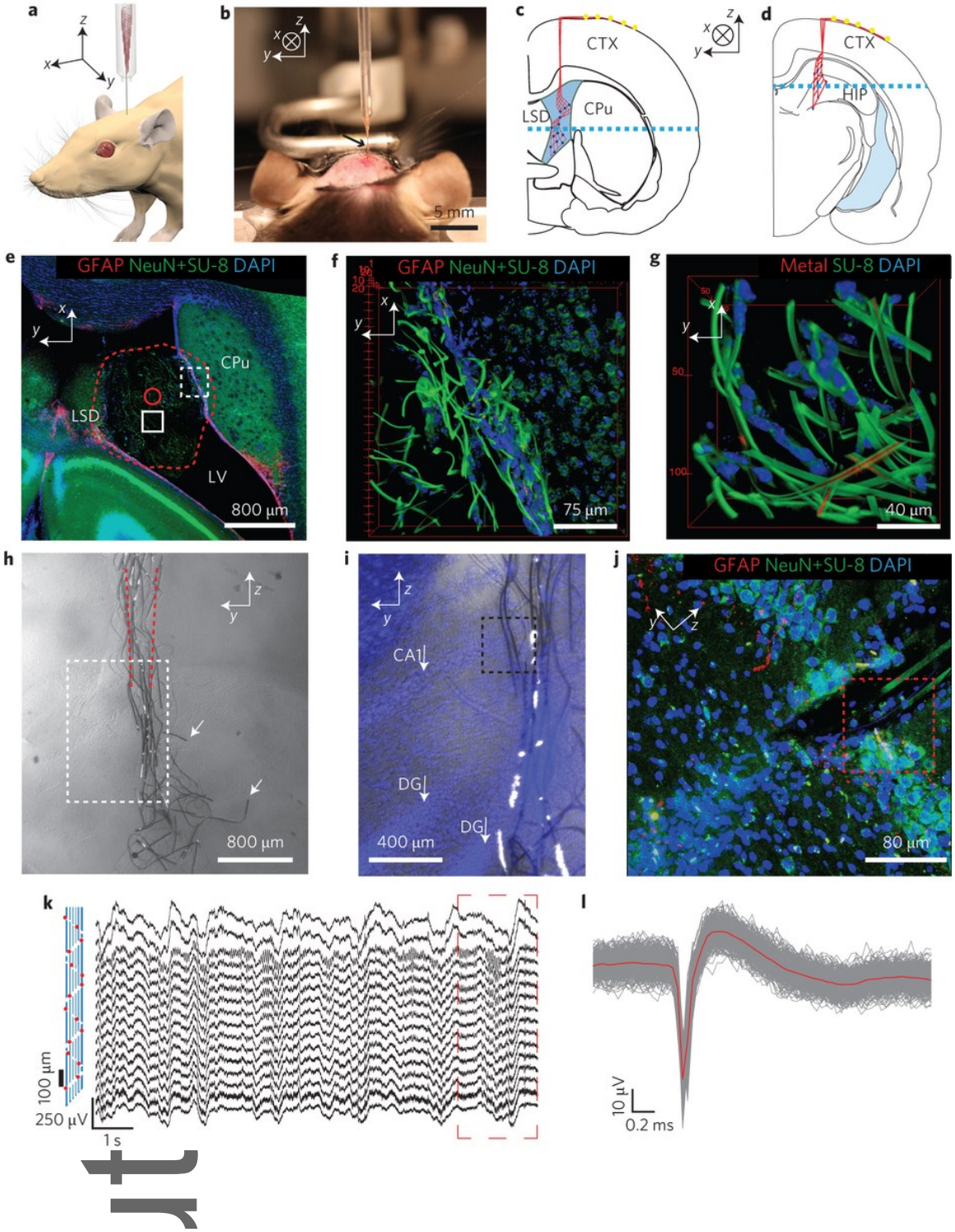

Figure 6. (a) Schematic shows in vivo stereotaxic injection of mesh electronics into a mouse brain. (b) Optical image of the stereotaxic injection of mesh electronics into an anaesthetized three-month-old mouse brain. (c-d) Schematics of coronal slices illustrating the two distinct areas of the brain into which mesh electronics were injected: through the cerebral cortex (CTX) and into the lateral ventricle (LV) cavity adjacent to the caudoputamen (CPu) and lateral septal nucleus (LSD) (c) and through the CTX into the hippocampus (HIP) (d). Red lines highlight and indicate the overall structure of the mesh, and dark blue filled circles indicate recording devices. The blue dashed lines indicate the direction of horizontal slicing for imaging. (e) Projection of the 3D reconstructed confocal image from a 100-µm-thick, 3.17-mm-long and 3.17-mm-wide volume horizontal slice five weeks

post-injection at the position indicated by the blue dashed line in **c**. The red dashed line highlights the boundary of the mesh inside the LV, and the solid red circle indicates the size of the needle used for injection. Red, green and blue colors correspond to GFAP, NeuN/SU-8 and DAPI, respectively, and are denoted at the top of the image panel in this and subsequent images. (f) 3D reconstructed confocal image at the interface between the mesh electronics and subventricular zone (SVZ). (g) 3D reconstructed confocal image at the approximate middle (of the *x*–*y* plane) of the LV in the slice. (h) Bright-field microscopy image of a coronal slice of the HIP region five weeks post-injection of the mesh electronics. Red dashed lines indicate the boundary of the glass needle. White arrows indicate longitudinal elements that were broken during tissue slicing. (i) Overlaid bright-field and epi-fluorescence images from the region indicated by the white dashed box in **h**. Blue corresponds to DAPI staining of the cell nuclei, and white arrows indicate CA1 and the dentate gyrus (DG) of the HIP. (j) Projection of the 3D reconstructed confocal image from a 30-μm thick, 317-μm-long and 317-μm-wide volume from the zoomed-in region highlighted by the black dashed box in **i**. (k) Acute in vivo 16-channel recording using mesh electronics injected into a mouse brain. The devices were Pt-metal electrodes (impedance ≈950 kΩ at 1 kHz) with their relative positions marked by red spots in the schematic (left panel), and the signal was filtered with 60 Hz notch during acquisition. The dashed red rectangle indicates the section used for spatiotemporal mapping of multichannel-LFP recordings. (l) Superimposed single-unit neural recordings from one channel after 300–6,000 Hz band-pass filtering. The red line represents the mean waveform for the single-unit spikes. Reproduced with permission.[181] Copyright 2015, Nature Publishing Group.

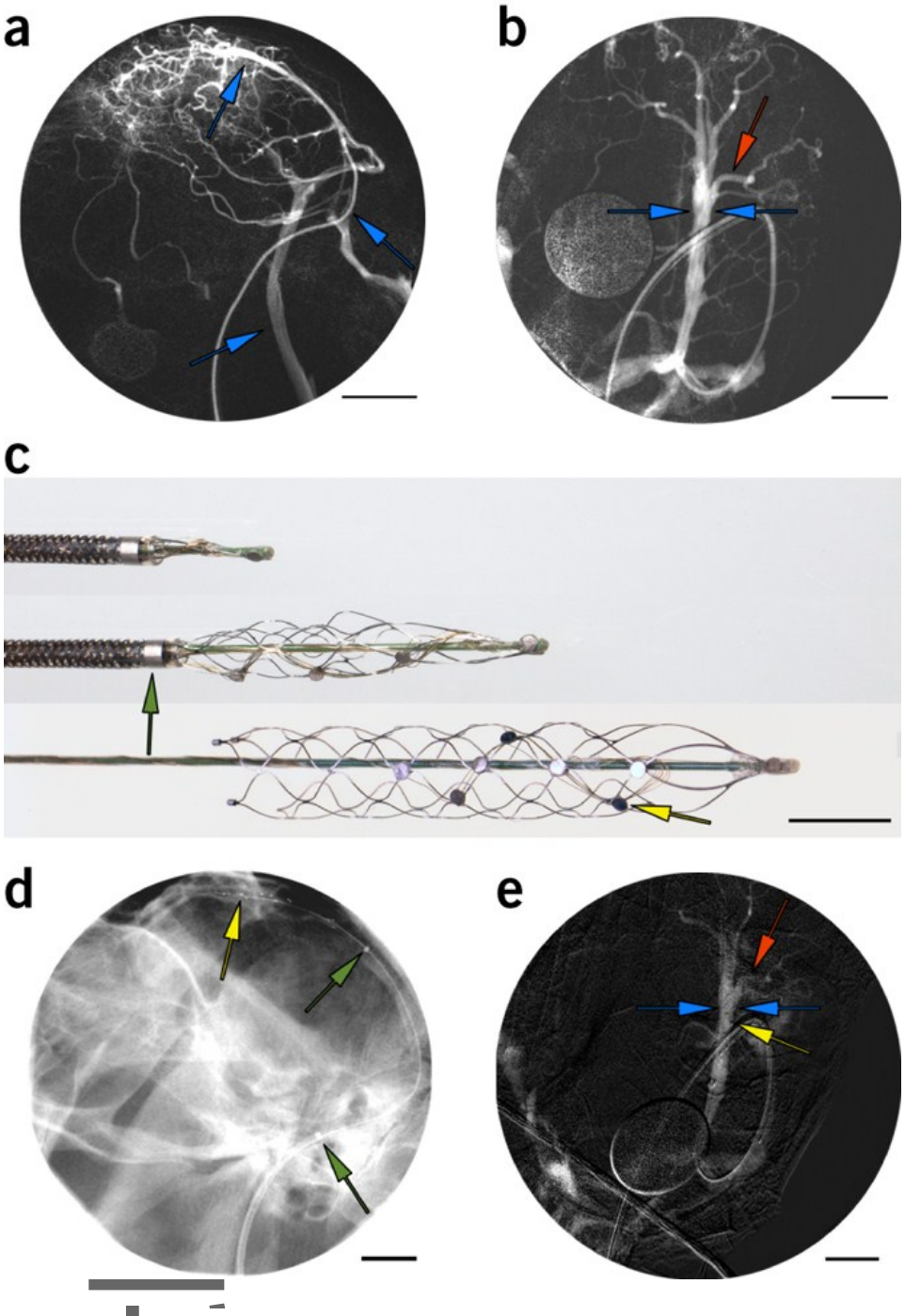

Figure 7. (a) Pre-implant lateral projection cerebral venography roadmap of external jugular vein, confluence of sinuses and superior sagittal sinus (SSS) (blue arrows). Scale bar, 20 mm. Circular artifact is a calibration tool. (b) Superior projection of SSS. Lumen diameter (blue arrows) and cortical veins (red arrow), assessed pre and post-implant. Scale bar, 10 mm. (c) Stentrode with 8 × 750 µm electrode discs (yellow arrow) self-expanding during deployment from 4F catheter (green arrow). Scale bar, 3 mm. (d) Post-implantation lateral projection plain X-ray of stentrode in SSS, displaying electrodes (yellow arrow) and delivery catheters (green arrows). Scale bar, 10 mm. (e) Post-implant superior projection contrast study of stentrode (electrodes, yellow arrow). Scale bar, 10 mm. Reproduced with permission.[183] Copyright 2016, Nature Publishing Group.

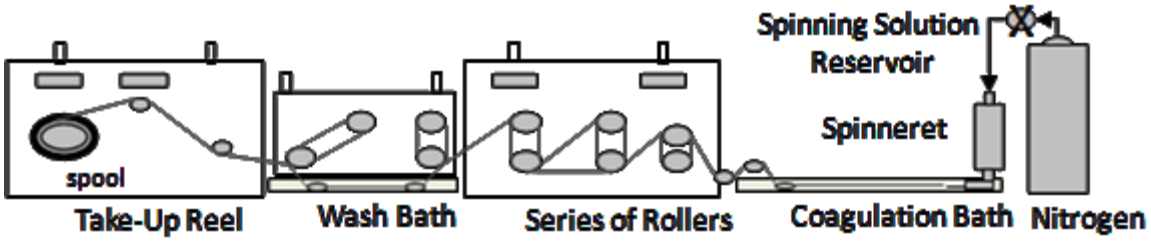

Figure 8. Spinning set up used to fabricate wet-spun polymer based fibers. Reproduced with permission.[84] Copyright 2012, Wiley-VCH.

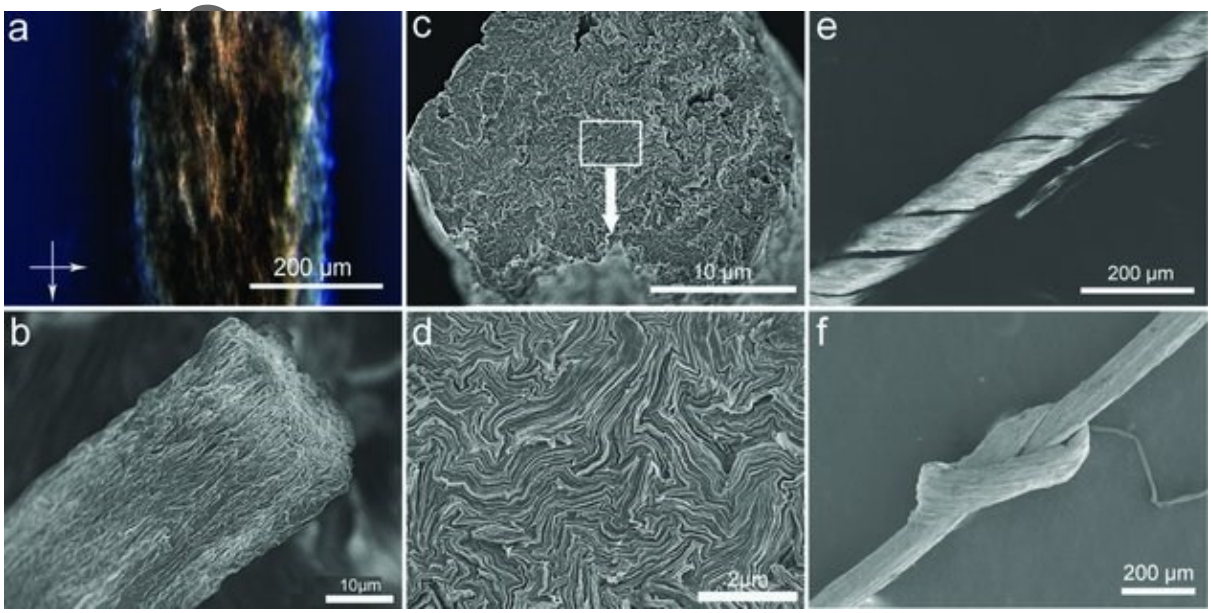

Figure 9. (a) Polarized optical microscopy image of as-spun gel-state GO fiber showing birefringence. Birefringence properties confirmed ordered LC domains were formed and preserved during spinning process (arrows show polarizers direction). SEM images of an as-spun GO fiber showing: (b) corrugated surface and (c) near-circular cross-section. (d) Close-up SEM image of the cross-section of GO fiber shown in b revealing GO sheet planes that are oriented along the fiber axis. (e-f) SEM images of crumpled and knotted rGO yarns (reduced by annealing) showing their flexibility. Reproduced with permission.[186] Copyright 2013, Wiley-VCH.

Biography

Alex Harris received his PhD from Monash University in electrochemistry under the supervision of Prof Alan Bond. Subsequently he was a team leader at Oxford Biosensors developing point-of-care blood sensors. He held a postdoctoral position at CSIRO, followed by a postdoctoral position at La Trobe University. He is currently a project leader in the HEARing CRC at the University of Wollongong. His research interest is in understanding and controlling electrode-tissue interfaces for bionics.

Gordon Wallace is currently the Executive Research Director at the ARC Center of Excellence for Electromaterials Science and Director of the Intelligent Polymer Research Institute. He previously held an ARC Federation Fellowship and currently holds an ARC Laureate Fellowship. Professor Wallace's research interests include organic conductors, nanomaterials and electrochemical probe methods of analysis, and the use of these in the development of Intelligent Polymer Systems. A current focus involves the use of these tools and materials in developing bio-communications from the molecular to skeletal domains in order to improve human performance via medical Bionics.

Table of Contents

Organic materials can control cell behavior; organic conducting materials are also able record and stimulate excitable cells. This review covers graphene, carbon nanotubes and organic conducting polymers interfacing with cells. Different methods of fabricating electrode structures are also discussed.

Keyword: Neural Electrodes

A. R. Harris*, G. G. Wallace*

Organic Electrodes and Communications with Excitable Cells